Ore Geology Reviews 64 (2015) 152–171

Contents lists available at ScienceDirect

Ore Geology Reviews

journal homepage: www.elsevier.com/locate/oregeorev

The trinity pattern of Au deposits with porphyry, quartz–sulfide vein and structurally-controlled alteration rocks in Ciemas, West Java, Indonesia

Zhengwei Zhang [a,*], Chengquan Wu [a,c], Xiaoyong Yang [b,*], Chaofei Zheng [a,c], Junhua Yao [a,c]

[a] State Key Laboratory of Ore Deposit Geochemistry, Institute of Geochemistry, Chinese Academy of Sciences, Guiyang 550002, China
[b] CAS Key Laboratory of Crust–Mantle Materials and Environments, School of Earth and Space Sciences, University of Science and Technology of China, Hefei 230026, China
[c] University of Chinese Academy of Sciences, Beijing 100049, China

ARTICLE INFO

Article history:
Received 25 January 2014
Received in revised form 2 July 2014
Accepted 3 July 2014
Available online 8 July 2014

Keywords:
Au deposit
Quartz–sulfide vein
Structure-controlled alteration rocks
Porphyry
Epithermal
Ciemas, West Java, Indonesia

ABSTRACT

The Ciemas gold mining area is located in the Sunda arc volcanic rock belt, West Java, Indonesia. Ore bodies are associated with Miocene andesite, dacite and quartz diorite porphyrite. To constrain ore genesis and mineralization significance, a detailed study was recently conducted examining these deposits, which included detailed field observation, petrographic study, petrochemistry, sulfur isotope analyses, zircon U–Pb dating, and fluid inclusion analysis. The results include the following findings. 1) Ore types have been identified as porphyry, a quartz–sulfide vein, and structure-controlled alteration rocks. 2) In host rocks, zircon LA–ICP-MS U–Pb dating of quartz diorite porphyrite, amphibole tuff breccia and andesite yield ages of 17.1 ± 0.4 Ma, 17.1 ± 0.4 Ma and 17.5 ± 0.3 Ma, respectively. 3) Fluid inclusions in the quartz from ore are given priority to liquid and gas–liquid phases, and their components are of the NaCl–H_2O system with homogenization temperatures of 240–320 °C, salinities of 14–17%, densities of 0.85–0.95 g/cm^3, and fluid pressure values between 4.1 and 46.8 MPa, corresponding to metallogenic depths from 150 to 1730 m. Fluid characteristics are identified as similar to those of high sulfur epithermal deposits. 4) The sulfur isotopic compositions are notably uniform, the $\delta^{34}S$ values of wall rocks range from 3.71 to 3.85‰, and the $\delta^{34}S$ values of ores vary from 4.90‰ to 6.55‰. The sulfur isotopic composition of ores is similar to that of the wall rocks, indicating a mixed origin of mantle with a sedimentary basement. 5) The trace element patterns of different ore types are similar, which indicates that they originate from the same source. Au deposits primarily occurred during the late magmatic activity. Finally, we have set up the regional metallogenic model, confirming that this gold deposit in the Sunda arc volcanic rock belt belongs to a metallogenic system from porphyry to epithermal type.

1. Introduction

The initial definition of epithermal deposition referred to deposition that occurs in a shallow place and always localizes to the volcanic rocks in low-temperature mineralized bodies (Lindgren, 1933), but with increased research, the connotation of this definition has changed. Buchanan (1981), based on the evolution of ore-forming fluid, established a comprehensive epithermal gold deposit model. Berger (1983) proposed the geological–geochemical concept model of the epithermal deposit. Bonham (1986) argued that this type of deposit could be divided into low-sulfur, high-sulfur and alkali rock types. Heald et al. (1987) divided the deposits into alunite–kaolinite and adularia–sericite types according to the ore mineral assemblages. Sillitoe (1997) suggested that epithermal deposits and porphyry deposits derived from the same thermal system and could occur at the same time. Hedenquist et al. (2000) suggested the intermediate-sulfide (IS) type between the high-sulfide (HS) and low-sulfide types (LS). Corbett (2002) tried to reveal the inner links between epithermal deposits, porphyry Cu–Au deposits and skarn deposits with a uniform model. Heinrich et al. (2004), Heinrich (2005) suggested that a steam cooling contraction mechanism led the ore-forming process from a porphyry copper–gold to an epithermal gold (copper) type. These facts illustrate that epithermal deposits are not limited to the low-temperature ranges and are closely associated with porphyry deposits and aspects of the mineralization and that they belong to a continuous series.

The Ciemas gold deposit is located in Sukabumi, West Java Province, Indonesia (Fig. 1a). Since 1980, many mining companies (including Parry Corporation Ltd., Terrex Resources NL, Meekatharra Minerals Indonesia and Wilton Wahana Indonesia) have implemented mineral exploration projects and resources (measured and indicated) of 16.5 t of gold metal have been delineated by exploration (Table 1). Since 2010, we have conducted an overall geological survey assessment based on exploration data and researched the mineral compositions, structures and geochemistry of mineral deposits. Altogether, some 10

* Corresponding authors.
E-mail addresses: zhangzhengw@hotmail.com (Z. Zhang), xyyang555@163.com (X. Yang).

http://dx.doi.org/10.1016/j.oregeorev.2014.07.003
0169-1368/

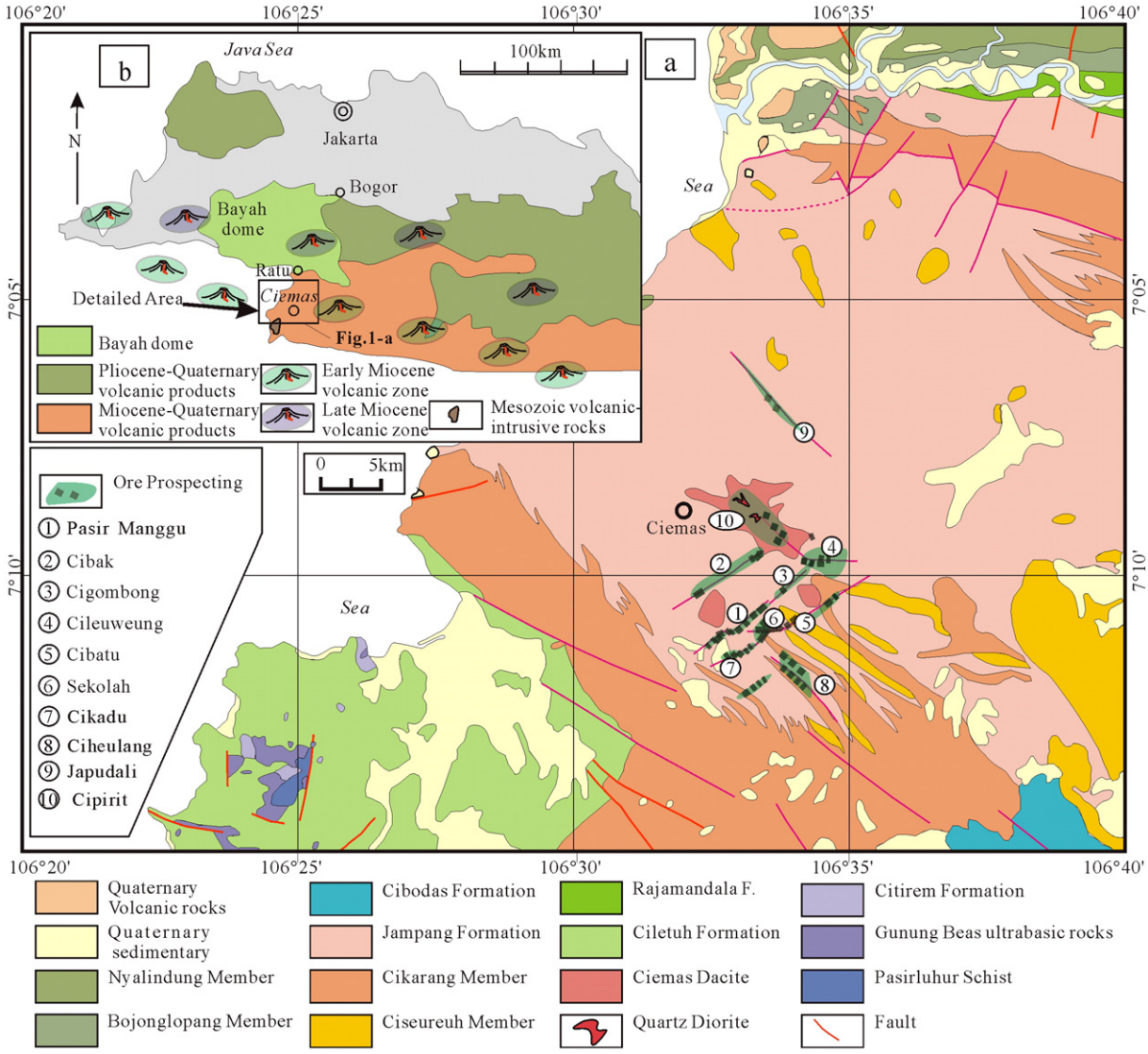

Fig. 1. a) Geological map showing the distribution of Au deposits in the Ciemas area, West Java, Indonesia (modified after Jonathan, 2007; Milesi et al., 1999; Sukamto, 1975). Deposit numbers and local names: 1 — Pasir Manggu; 2 — Cibak; 3 — Cigombong; 4 — Cileuweung; 5 — Cibatu; 6 — Sekolah; 7 — Cikadu; 8 — Ciheulang; 9 — Japudali; 10 — Cipirit. b) Map of West Java showing the location of the Ciemas deposit hosted by the late Eocene to early Miocene volcanic rock belt.

gold deposits have been discovered in the range of 10 km^2 (Hong et al., 2013). We suggest that the genesis of these deposits is closely related to the magmatic hydrothermal activity whereby Miocene quartz diorite porphyrite intruded into andesite and dacite, from the perspective of ore-forming space and time. Both similarities and differences are relative to some typical porphyry–epithermal deposits (Corbett, 2002; Marcoux and Milési, 1994). Ore types include porphyry, quartz–sulfide vein (equivalent to the high-sulfur type) and structurally controlled alteration rocks near the porphyry intrusion. Topographically, the lower of the ore bodies is a quartz–sulfide vein, and the upper is carbonate-base metal, with the spatial distribution of ore bodies being similar to that of low-sulfur types. Because of these characteristics, the Ciemas gold deposit is considered a special porphyry–epithermal system related to the magmatic arc background (Fig. 1b), which deserves detailed research work. In this paper, taking the Ciemas gold deposit as an example, we propose the spatial concept model of the trinity according to the interconnection of different ore bodies in terms of space and origin.

From the center to the periphery of the hypabyssal intrusions, the gold mineralization successively evolved from porphyry type to sulfide type with quartz vein-structurally-controlled vein type. Differences in the ore types are closely related to magmatic temperature and the degree of mixing between magmatic fluids and meteoric water.

2. Geological background

2.1. Tectonic setting

The Ciemas Au deposit is situated within West Java at the southern margin of Sundaland (Fig. 1), which is the continental core of SE Asia formed by the accretion of blocks to the Eurasian margin (Hall, 2002; Hamilton, 1988), and was assembled by the time of the Late Triassic (Clements and Hall, 2007, 2008). Volcanic rocks (Citirem Formation) and metamorphic rocks (Pasrluhur schist) of Mesozoic age exposed in southern Ciemas (Fig. 1a) were accreted at the periphery of Sundaland in West Java (Wakita, 2000). By the end of the Cretaceous and during the Paleocene, much of Sundaland was an emergent continental region, most likely with a passive margin in southern Java (Carlile and Mitchell, 1994). However, rapid northward movement of the Australian Plate occurred in the Eocene. Northward subduction of the Indo-Australian Plate beneath the Eurasian Plate has most likely been continuous since

the early Paleogene, although associated volcanism may not have been continuous (Hamilton, 1989; Hutchison, 1988). Almost all of the rocks exposed on Java are Cenozoic, and they include igneous intrusions, volcanic products, siliciclastic sedimentary rocks and shallow marine carbonates (Claproth, 1989; Katili, 1989; Van, 1970; Whitford et al., 1979). The Ciemas gold deposit is hosted by a late Eocene to early Miocene volcanic rock belt (Fig. 1b).

2.2. Sedimentary lithostratigraphy

In the mining area, except for a tiny amount of Mesozoic units, most rocks are exposed Tertiary volcanic breccia, tuff and andesite, as well as Quaternary residual deposits and alluvial deposits (Jonathan, 2007; Milesi et al., 1999; Sukamto, 1975). The regional strata are described in Fig. 1a and Table 2.

2.3. Structure

The regional structure has two sets of main orientations to faults, i.e., the NE strike and NW strike (Fig. 1a). The fold mainly consists of the Ciemas syncline, which is a similar fold with a NE axial direction. The main faults constituting the ore body are (Fig. 1a) detailed as follows: (1) The Japudali fault has an NW strike (310°), a NE dip with a high angle (60°–70°) and is more than 1000 m in length and 30 m wide. The structurally controlled alteration rocks, consisting of volcanic breccia and argillaceous altered rocks, are visible within the fault with pyrite and chalcopyrite. (2) The Pasir Manggu fault has a NE strike (45°), a SE dip with a high angle (60°–70°) and is more than 1000 m in length and 30 m wide. The structural fracture zone consists of volcanic breccia, quartz veins and argillaceous altered rocks, including a chalcedony–quartz vein with pyritization (Fig. 2). (3) The Cibatu fault presents a NE strike (50°), a NW dip with a high angle (60°–80°) and is more than 2000 m in length and 20 m wide. The structurally controlled alteration rocks consist of volcanic breccia, and altered argillaceous rocks are visible within the fault with silicide and lead–zinc–copper mineralization (Fig. 2). (4) The Ciheulang fault has a NW strike (320°), a NE dip with a high angle (60°–80°) and is more than 1000 m in length and 30 m wide (Fig. 2). The structurally controlled alteration rocks consist of volcanic breccia, and altered argillaceous rocks are visible within the fault zone with silicide, pyrite, chalcopyrite and lead–zinc mineralization.

According to the structural analysis, the ore-bearing faults represent three periods of tectonic activity. Early activity in the extensional fault is shown in the stockwork and filling structure. The middle activity is indicated by the compressional fault with shear alteration consisting of the schistosity of tectonic schist and fracture breccia, and the late activity is represented by the extensional fault with a gold-bearing fractured zone with a chalcedony–quartz vein, silicification, pyritization and carbonatization.

2.4. Igneous rocks

A large number of scattered dacites for a diameter of several kilometers are characterized by rich double-cone coarse quartz. Few intrusions are exposed. Only one dacite has been found within the Ciemas region. Small amounts of Mesozoic basic–ultra-basic rocks and Pasirluhur schist outcrop in the mining area 30 km away (Fig. 1a).

In Cipirit, a quartz diorite porphyrite intrudes into the Miocene dacite and andesite, consisting of mid-coarse quartz and hornblende phenocrysts in a matrix of primarily cryptocrystalline quartz and feldspar. The rock mass outcrops as stocks, which have propylitization at the top and side, and mineral composition mainly includes chlorite, epidote, quartz, calcite and pyrite and chalcopyrite (Fig. 3a-1). The rock has a massive structure and a porphyritic texture, with chalcopyrite and pyrite on the edge of hornblende phenocrysts or in the matrix (Fig. 4b).

3. Deposit descriptions

The mining area can be divided into 10 ore blocks (Fig. 1, Table 1), and the mineralized rock types are described in the following subsections.

3.1. Quartz–sulfide vein ore deposits

Four ore blocks, Pasir Manggu, Cigombong, Cileuweung and Cibak, are of the quartz vein type (Fig. 2). Among them, the Pasir Manggu ore block has been extensively explored (Fig. 5a, b). As a typical ore deposit, its details follow (the features of the other three ore blocks are briefly described in Table 1).

The Pasir Manggu mining area is distributed in the Miocene Jampang Formation composed of andesite lava, breccia and volcanic clastic rock (Fig. 5a). The exposed Cibak and Cibatu dacites are nearby, with a developed NNE fault zone (Fig. 2). The orebody consists of chalcedony, andesitic breccia with quartz cementation and quartz veins in the structure alteration zones (Fig. 5a) with an average 45° direction. The drill spacing is on approximately 20 × 20 m grids over approximately 640-m-long controlled orebodies occurring in layered veins (Fig. 3b) that dip SE at angles of 75° to 80°, extending to a depth of 60–120 m (Fig. 5b). The tops and bottoms of the orebodies are composed of andesitic breccia. Gold grades in the horizontal and vertical planes have certain changes, especially where the NE–NW fractures cross, and the ore body becomes thicker with high grades. There are two main orebodies (Fig. 5): 300–650 m long, 1–7.50 m thick, gold grade 1–22.60 g/t, average grade of 6.88 g/t, and 2.65 t of gold metal resources.

The metal ore minerals are pyrite, chalcopyrite, arsenopyrite, marcasite, limonite and arsenic sulfide copper ore. The gangue minerals include quartz, plagioclase, chlorite, epidote, sericite, biotite, clay, calcite, dolomite, and ankerite. In addition to gold, the orebodies also contain associated Ag (10 to 60 g/t, highest Ag grade 512 g/t). The mineral paragenetic association is mainly pyrite, natural gold and quartz.

Ore textures are the fine-grained type, euhedral–half-euhedral granular types and poikilitic type, with structures of disseminated type, fine veins and disseminated and massive types. The ore types are oxidized ores on the surface and sulfide ores in the depth. The oxidation zone ranges from 5 to 10 m in depth. In the original sulfide ores, the metal minerals are pyrite, marcasite, arsenic pyrite, galena, sphalerite, chalcopyrite, argentite, gold and silver. The gold-to-silver ratio is 4:1 with an average arsenic content of 0.70%, a lead content of 0.05% and a zinc content of 0.06%. The gold occurs in the edges of base metal sulfides or dissolved in arsenopyrite or is in the quartz. The gold particle size is usually 2–40 μm.

Three periods of the mineralization process have been identified: 1) the first period is characterized by a banded chalcedony-silicide, generally without gold mineralization; 2) the second period is characterized by an arsenic pyrite quartz vein and brecciated process; 3) the third period is characterized by ore-bearing hydrothermal filling metasomatism forming banded structures of chalcedony cements and sulfide, and intergrowth of precious metal ores. The wall rock alteration displays strong argillic alteration (mainly kaolinite, illite and montmorillonite), and the thickness of the alteration zone is up to 5 m in the top of ore body, becoming narrow on the footwall (Fig. 3b).

3.2. Ore deposits of structurally-controlled alteration rocks

The structurally-controlled deposits are mainly Ciheulang, Cibatu, Cikadu, Sekolah and Japudali. Among them, the Cibatu mine, as a typical ore deposit, is described below (characteristics of the other deposits are briefly summarized in Table 1).

The Cibatu mining area is distributed in the Miocene Jampang Formation composed of the Cikarang Member and Ciseureuh Member. The exposed Cibatu dacite is nearby, with a developed NNE direction fault zone composed of cataclastic rock, schist and silicide, mud and

Table 1
Characteristics of Au–Ag–multimetal deposits in the Ciemas, west Java, Indonesia.

Deposit No. longitude, latitude Location	Ore type and Ore-forming element association Au Resources	Ore body morphology and position within host rocks	Mineral association within ore body	Structure and texture of ores	Natural type of ore and grade of ore	Host rock and altered wall rock	Ore-controlling structures
No. 1 Pasir Manggu 106°32′35″, 07°11′12″ Sukabumi County	Quartz vein (Au, Ag), Au 2.642 t/measured 2.186 t/indicated 1.303 t/inferred	Multiple quartz vein zone within fault, presenting as compound vein. Average strike NNE 45°, dip direction SE, dip angle 75° to 80°, extending to the deep, tilting generally 60–120 m, length 640 m with thickness of 1–7.50 m. Total four gold ore bodies are explored	Mainly pyrite, As-bearing pyrite, and pyrrhotite, with minor chalcopyrite, marcasite, limonite. Secondary ilmenite, hematite and covellite. Gangue minerals including quartz, plagioclase, chlorite, epidote, sericite, biotite, clay, calcite, dolomite, ankerite	Idiomorphic granular texture, replacement texture and poikilitic texture. Mainly brecciated, disseminated, mesh-vein structure, with minor colloform, massive structure. Assemblages of pyrite–native gold–quartz	Oxidized ore and sulfide ores, oxidation zone generally deep 5–10 m. Gold grade 1–22.6 g/t, the average grade of 6.88 g/t	Jampang Formation andesitic lava, breccia, and volcaniclastic rock. Hanging wall and foot wall of ore body within andesitic volcanic breccia, with strong clay mineralization, alteration belt thickness 5–10 m	Nearby Cibak dacite, ore hosted fault strike NE. Fault activity through the tensile, compressor-shear and tensile-shear process
No. 2 Cigombong 106°34′08″, 07°10′02″ Sukabumi County	Quartz vein (Au, Cu), Au 3.38 t/inferred	Massive quartz occurs as veins within altered dacite. Orebody's dip direction is 350° dip angle 60°, with length 500 m, thickness 1–10 m, deep unknown. Total six gold ore bodies are explored	Mainly pyrite, As-bearing pyrite, and pyrrhotite, with minor chalcopyrite, marcasite, limonite. Secondary ilmenite, hematite and covellite. Gangue minerals including quartz, plagioclase, chlorite, epidote, sericite, biotite, clay, calcite, dolomite, ankerite	Idiomorphic granular texture, replacement texture and poikilitic texture. Mainly brecciated, disseminated, mesh-vein structure, with minor colloform, massive structure. Assemblages of pyrite–native gold–quartz. Assembly pyrite–native gold–quartz	Oxidized ore and sulfide ores, oxidation zone generally deep 5–10 m. Gold average grade of 5.49 g/t	Ciemas dacite and Jampang Formation andesitic lava. Hanging wall and foot wall of ore body within andesitic volcanic breccia, with strong clay mineralization, alteration belt thickness 5–10 m	Nearby Ciemas dacite, ore hosted fault strike NW, intersection with propylitization zone. Fault activity appears as expanding, occurs the crystal class quartz
No. 3 Cileuweung 106°34′30″, 07°09′53″ Sukabumi County	Quartz vein (Au, Cu), Au 3.33 t/inferred	Open growth quartz vein with geode, occurs as veins within altered dacite, orebody as dip direction NW, dip angle 45°–60°, with length 100–500 m, thickness 1–3 m, deep unknown	Mainly pyrite, As-bearing pyrite, and pyrrhotite, with minor chalcopyrite, marcasite, limonite. Secondary ilmenite, hematite and covellite. Gangue minerals including quartz, plagioclase, chlorite, epidote, sericite, biotite, clay, calcite, dolomite, ankerite	Idiomorphic granular texture, replacement texture and poikilitic texture. Mainly brecciated, disseminated, mesh-vein structure, with minor colloform, massive structure. Assemblages of pyrite–native gold–quartz. Assembly pyrite–native gold–quartz	Oxidized ore and sulfide ores, oxidation zone generally deep 5–10 m. Gold grade 1–20.43 g/t, the average grade of 11.47 g/t	Jampang Formation andesitic lava, breccia, and volcaniclastic rock. Hanging wall and foot wall of ore body within andesitic volcanic breccia, with strong clay mineralization, alteration belt thickness 5–10 m	Nearby Cipiri dacite, ore hosted fault strike NE, intersection with propylitization zone. Fault activity appears as expanding, occurs the crystal class quartz
No. 4 Cibak 106°32′45″, 07°09′56″ Sukabumi County	Quartz vein (Au, Ag, Pb, Zn), Au 6.96 t/inferred	Quartz–quartzite-argillization zone within fault. Orebody as dip direction 315°, dip angle 60°, with length 800 m, thickness 0.5–4 m, deep unknown. Total three gold ore bodies are explored	Mainly pyrite, As-bearing pyrite, and pyrrhotite, with minor chalcopyrite, marcasite, limonite. Secondary ilmenite, hematite and covellite. Gangue minerals including quartz, chlorite, sericite, biotite, clay, calcite, dolomite, ankerite	Idiomorphic granular texture, replacement texture and poikilitic texture. Mainly brecciated, disseminated, mesh-vein structure, with minor massive structure. Assembly pyrite–native gold–quartz. Assemblages of pyrite–native gold–quartz	Oxidized ore and sulfide ores, oxidation zone generally deep 5–10 m. Gold grade 1–16.43 g/t, the average grade of 8.40 g/t	Jampang Formation andesitic lava, breccia, and volcaniclastic rock. Hanging wall and foot wall of ore body within andesitic volcanic breccia, with strong clay mineralization, alteration belt thickness 5–10 m	Nearby Cibak dacite, ore hosted fault strike NE, intersection with alteration belt. Fault activity appears as expanding, occurs the crystal class quartz
No. 5 Cibatu 106°33′57″, 07°10′51″ Sukabumi County	Structural alterated rock (Au, Pb, Zu), Au 4.595 t/indicated; 3.715 t/inferred	Along the structure-controlled alteration zone appears in bedded, veined and irregular ore bodies, dip direction 330°, dip angle 60° to 65°, extending to the deep in the tilt generally 80–130 m, length 700 m, thickness 1–8 m. Total three gold ore bodies are explored	Mainly pyrite, sphalerite, galena, and pyrrhotite, with minor chalcopyrite, marcasite. Secondary limonite, malachite and hematite. Gangue minerals including quartz, chlorite, epidote, sericite, clay, calcite	Granules crystalloblastic texture, cataclastic texture and lepidoblastic texture. Mylonitic structure, schistose structure, partly mesh-vein structure. Assemblages of galena–native gold–quartz–pyrite	Oxidized ore and sulfide ores, oxidation zone generally deep 5–10 m. Gold grade 1–10.32 g/t, the average grade of 6.73 g/t	Jampang Formation, Cikarang Member and Ciseureuh Member. Hanging wall and foot wall of ore body within andesitic volcanic breccia, alteration with mainly chloritization and pyritization, secondly silicification, carbonation and epidotization	Nearby Cibatu dacite, ore hosted fault strike NE. Fault activity through the tensile, compressor-shear and tensile-shear process

(continued on next page)

Table 1 (*continued*)

No. 6 Sekolah 106°33′27″, 07°10′58″ Sukabumi County	Structural alterated rock (Au, Fe), Au 1.361 t/indicated 7.043 t/inferred	Along the structure-controlled alteration zone appears in bedded, veined and irregular ore bodies, dip direction 330°, dip angle 60° to 65°, extending the deep in the tilt generally 80–130 m, length 920 m, thickness 1–8 m. Total three gold ore bodies are explored	Mainly pyrite, sphalerite, galena, and pyrrhotite, with minor chalcopyrite, marcasite. Secondary limonite, malachite and hematite. Gangue minerals including quartz, chlorite, epidote, sericite, clay, calcite	Granules crystalloblastic texture, cataclastic texture and lepidoblastic texture. Mylonitic structure, schistose structure, partly mesh-vein structure. Assembly galena–native gold–quartz–pyrite	Oxidized ore and sulfide ores, oxidation zone generally deep 5–10 m. Gold grade 1–18.44 g/t, the average grade of 7.41 g/t.	Jampang Formation, Cikarang Member and Ciseureuh Member. Hanging wall and foot wall of ore body within andesitic volcanic breccia, alteration with mainly chloritization and pyritization, secondly silicification, carbonation and epidotization	Nearby Cibatu dacite, ore hosted fault strike NE. Fault activity through the tensile, compressor-shear and tensile-shear process
No. 7 Cikadu 106°32′52″, 07°11′22″ Sukabumi County	Structural alterated rock (Ag, Fe), Au 5.745 t/indicated 3.698 t/inferred	Along the structure-controlled alteration zone appears in bedded, veined and irregular ore bodies, dip direction 330°, dip angle 60° to 65°, extending the deep in the tilt generally 80–130 m, length 840 m, thickness 1–8 m. Total three gold ore bodies are explored	Mainly pyrite, sphalerite, galena, and pyrrhotite, with minor chalcopyrite, marcasite. Secondary limonite, malachite and hematite. Gangue minerals including quartz, chlorite, epidote, sericite, clay, calcite	Granules crystalloblastic texture, cataclastic texture and lepidoblastic texture. Mylonitic structure, schistose structure, partly mesh-vein structure. Assemblages of galena–native gold–quartz–pyrite	Oxidized ore and sulfide ores, oxidation zone generally deep 5–10 m. Gold grade 1–10.30 g/t, the average grade of 8.99 g/t.	Jampang Formation, Cikarang Member and Ciseureuh Member. Hanging wall and foot wall of ore body within andesitic volcanic breccia, alteration with mainly chloritization and pyritization, secondly silicification, carbonation and epidotization	Nearby Cibatu dacite, ore hosted fault strike NE. Fault activity through the tensile, compressor-shear and tensile-shear process
No. 8 Ciheulang 106°34′05″, 07°11′47″ Sukabumi County	Structural alterated rock (Ag, Fe), Au 4.78 t/inferred	Along the structure-controlled alteration zone appears in bedded, veined and irregular ore bodies, dip direction NE, dip angle 68°, length 200 m, thickness 2–4 m, extending deep unknown. Only one gold ore body is explored	Mainly pyrite, sphalerite, galena, and pyrrhotite, with minor chalcopyrite, marcasite. Secondary limonite, malachite and hematite. Gangue minerals including quartz, chlorite, epidote, sericite, clay, calcite	Granules crystalloblastic texture, cataclastic texture and lepidoblastic texture. Mylonitic structure, schistose structure, partly mesh-vein structure. Assemblages of galena–native gold–quartz–pyrite	Oxidized ore and sulfide ores, oxidation zone generally deep 5–10 m. Gold grade 5–30 g/t	Jampang Formation, Cikarang Member and Ciseureuh Member. Hanging wall and foot wall of ore body within andesitic volcanic breccia, alteration with mainly chloritization and pyritization, secondly silicification, carbonation and epidotization	Nearby Cibatu dacite, ore hosted fault strike NW. Fault activity through the tensile, compressor-shear and tensile-shear process
No. 9 Japudali 106°33′05″, 07°06′27″ Sukabumi County	Structural alterated rock (Au, Pb, Zu), Au 13.92 t/inferred	Along the structure-controlled alteration zone appears in bedded, veined and irregular ore bodies, dip direction NE, dip angle 70°–70°, length 300 m, thickness 2–4 m, extending deep unknown. Total four gold ore bodies are explored	Mainly pyrite, sphalerite, galena, and pyrrhotite, with minor chalcopyrite, marcasite. Secondary limonite, malachite and hematite. Gangue minerals including quartz, chlorite, epidote, sericite, clay, calcite	Granules crystalloblastic texture, cataclastic texture and lepidoblastic texture. Mylonitic structure, schistose structure, partly mesh-vein structure. Assembly galena–native gold–quartz–pyrite	Oxidized ore and sulfide ores, oxidation zone generally deep 5–10 m. On the earth's surface, gold grade 8.46 g/t; in tunnel, gold grade 7.70 g/t.	Jampang Formation andesitic lava, breccia, and volcaniclastic rock. Hanging wall and foot wall of ore body within andesitic volcanic breccia, alteration with mainly chloritization and pyritization	Ore hosted fault strike NW. Fault activity through the tensile, compressor-shear and tensile-shear process
No. 10 Cipirit 106°33′05″–03″, 07°08′46″ Sukabumi County	Porphyry Pb–Zu (Au, Cu), Au 19.91 t/inferred	In outer of porphyry appears in bedded, veined and irregular ore bodies, single length 20–80 m, thickness 3–10 m, deep 50 m. In dacite presenting as stockworks quartz vein	Mainly pyrite, chalcopyrite, pyrrhotite, magnetite, sphalerite and galena, with minor arsenopyrite, marcasite, limonite. Secondary bornite, ilmenite, hematite and covellite. Gangue minerals including quartz, sericite, chlorite and calcite	Idiomorphic–xenomorphic crystal texture, interstitial, metasomatic, poikilitic texture, and myrmekitic texture. Banded, disseminated, massive, mesh-vein structure, and brecciated structures. Assemblages of pyrite–native gold–quartz–chalcopyrite	In propylitization belt, with pyrite, magnetite and native gold, oxidation zone generally deep 5–10 m, the average gold grade of 1.22 g/t.	Ciemas Dacitec, quartz diorite porphyrite, with strong propylitization, with epidote, chlorite, albite, and carbonation (calcite, dolomite and ankerite), with minor sericitization	Ciemas Dacitec covering on Jampang Formation andesite, and quartz diorite porphyrite intruded into Ciemas dacite. Ore hosted fault strike NE, intersection with propylitization belt

The ore deposit characteristics are compiled based on Jonathan (2007); Hong et al. (2013). In the table "Deposit no." is the same as in Fig. 1.

Table 2
Sedimentary lithostratigraphy of the host rocks for the Au–Ag polymetallic deposits in the Ciemas area, West Java, Indonesia (modified after Sukamto, 1975).

	Formation	Member	Lithological description
Quaternary			A series of deposits consist of andesite, volcanic breccia, alluvium and coastal deposits, Citanglar beach deposits, young terrace deposits, old terrace deposits and coral reef limestone
Miocene	Cibodas		Limestone, tuffaceous limestone, sandy limestone, with intercalation of calcareous sandstone and tuffaceous sandstone
Miocene		Bojonglopang	Coral/globigerina/bioclastic/sandy limestone with intercalation of marls, sandstone, claystone, conglomerate at base and coal lenses
Miocene		Nyalindung	Claystone mudstone and sandy claystone with intercalation of sandstone and marl
Miocene	Jampang		The lower part consists of globigerina marl, sandstone and calcareous brecciated tuff of andesitic and dacitic composition with intercalation of thick limestone beds containing larger foraminifers. The upper part consists of volcanic breccia tuff and locally contains nodules and lenses of limestone with many andesitic to dacitic sills, dikes, stocks and quartz veins
Miocene		Cikarang	Tuff and lapilli tuff, interbedded with pumice tuff, pumice sandstone, calcareous sandstone, pumiceous, andesitic, dacitic, and brecciated tuff. The lower part contains calcareous tuffaceous sandstone, lapilli tuff and calcareous breccia. The upper part consists of marl, limestone, pumiceous tuff, tuffaceous sandstone and tuffaceous marl
Miocene		Ciseureuh	Andesite and basaltic lava flows, partly brecciated pillow basalts
Oligocene	Rajamandala		Tuffaceous marl, marly claystone, tuff sandstone, and reef and clastic limestones, party marbleized type
Eocene	Ciletuh		Quartz sandstone, quartz conglomerate, gray claystone, shale and slate, intercalations of greywacke and polymictic breccia
Mesozoic	Citirem		Diabase and basalt, syenite, andesite and spillite, in the forms of lava flows, partly with brecciated type, locally with pillow structure, altered and hydrothermal alteration

carbonate alteration along structurally-controlled rocks (Fig. 2). The orebody occurs in deformed rocks (Fig. 6a), extends to a length of 350–700 m, and a thickness of 1.8 m and is dipping 330° at a 60° angle. Ore bodies are in vein form with a layered outcrop and are consistent with the occurrence of a tectonic fracture zone with a dipping extension 80–130 m in length. The top and bottom rocks of the ore

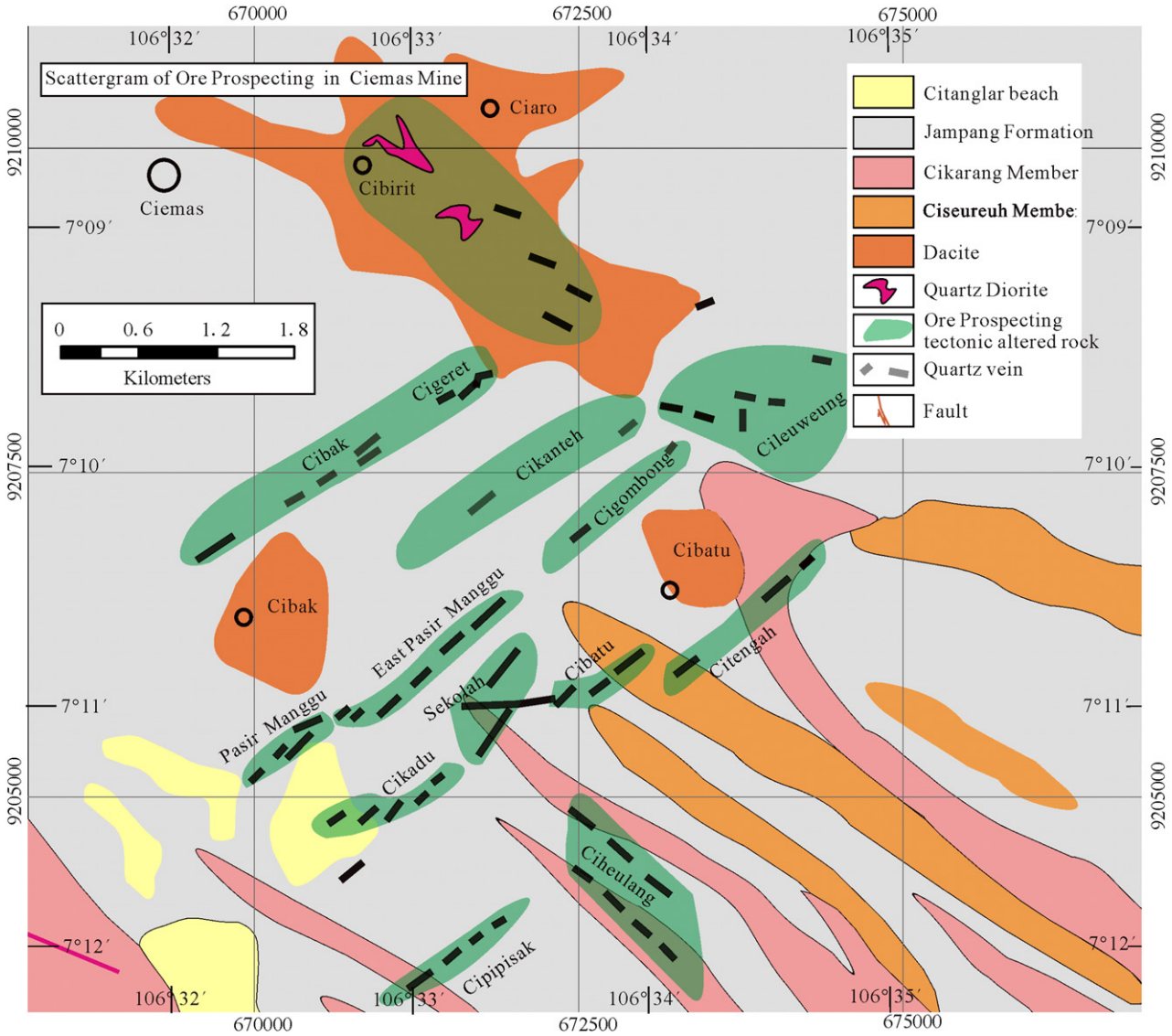

Fig. 2. Simplified geological map of the Ciemas area showing the location of the 10 main veins of the deposit (modified after Jonathan, 2007).

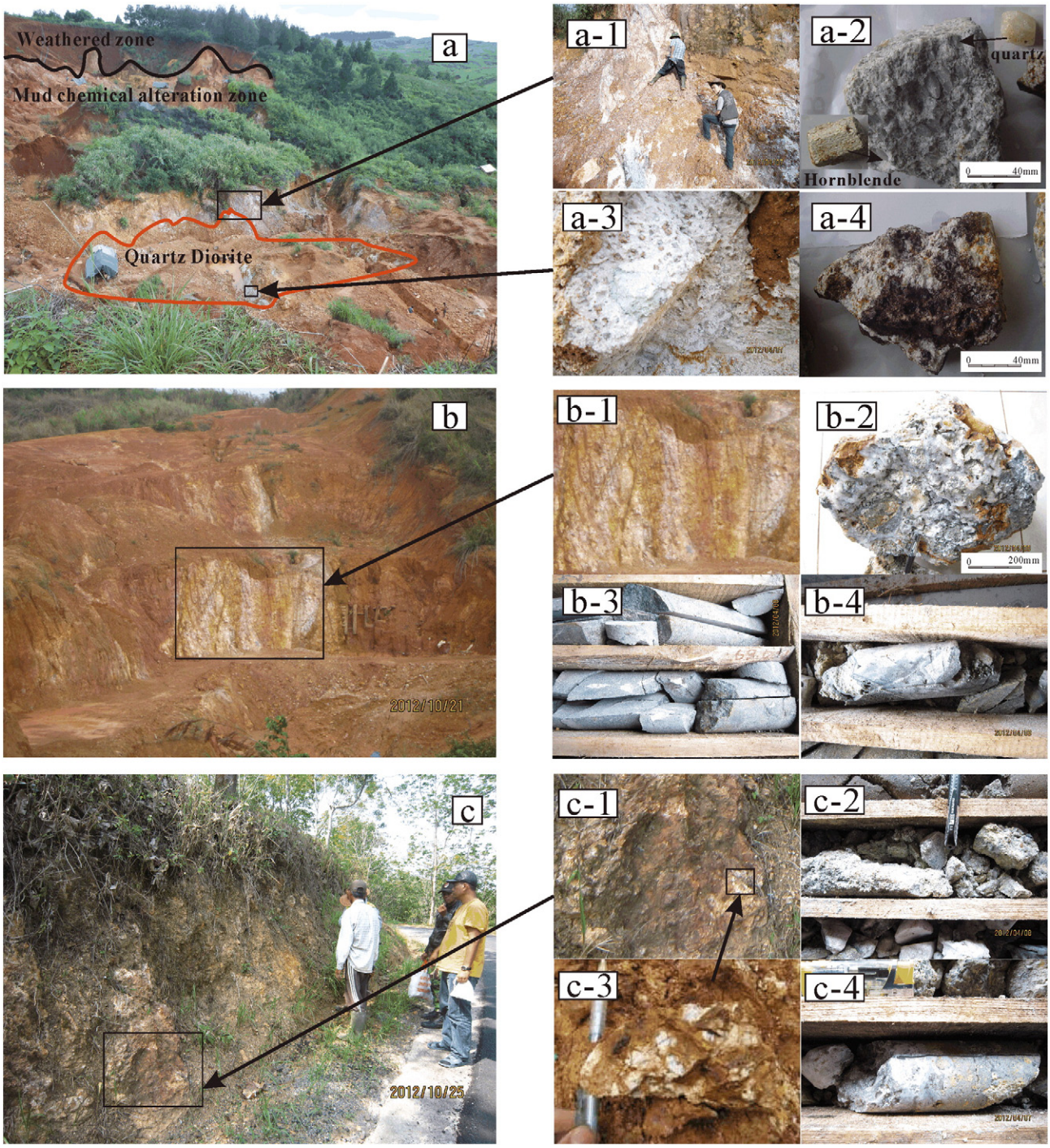

Fig. 3. Photos of orebody outcrops, ore textures and structures from the Cipirit (a), Pasir Manggu (b) and Cibatu (c) deposits. a-1 dacite intercalation of quartz diorite porphyrite; a-2 quartz diorite porphyrite; a-3 hexagonal bipyramidal quartz phenocryst, rhombic prism of phenocryst of hornblende and pyrite within quartz diorite porphyrite; a-4 silication and limonitic gold ore; b-1 ore body within multiple quartz vein zone; b-2 brecciated ore, andesite, quartz and chalcedony; b-3 carbonatization within andesite; b-4 silication, carbonatation and pyritized ore; c-1 brecciation and mylonitization in a structurally-controlled alteration belt; c-2 pyrite ore within an argillization belt; c-3 carbonatation and silication within a structurally-controlled alteration belt; c-4 Silication, carbonatation and pyrite ore within an argillization belt.

body are altered andesite (Fig. 6b). The drill spacing is approximately 40 × 40 m grids with many drill holes, and there are three controlled orebodies with 4594 kg of gold metal reserves with gold grades of 1.00–20.32 g/t (average grade of 6.37 g/t).

The ore minerals are mainly pyrite, limonite, galena, sphalerite, chalcopyrite and malachite. The gangue minerals are quartz, sericite, chlorite and calcite. The ores have granular blastic texture, cataclastic structure, and block and flake structures. Pyrite is often dotted along the fractures of cataclastic rocks or structural surface of mylonite, forming irregular veins.

The ore types are pyrite, limonite and malachite in altered andesite. Because of the development of schistosity and fractures in altered rocks, the degree of ore oxidation is higher, and the oxidation depth can reach approximately 60 m. The surface rock is chlorite schist with limonitization, and the deep rock is chlorite schist with pyritization. The tectonically altered rocks of the ore bodies are located only

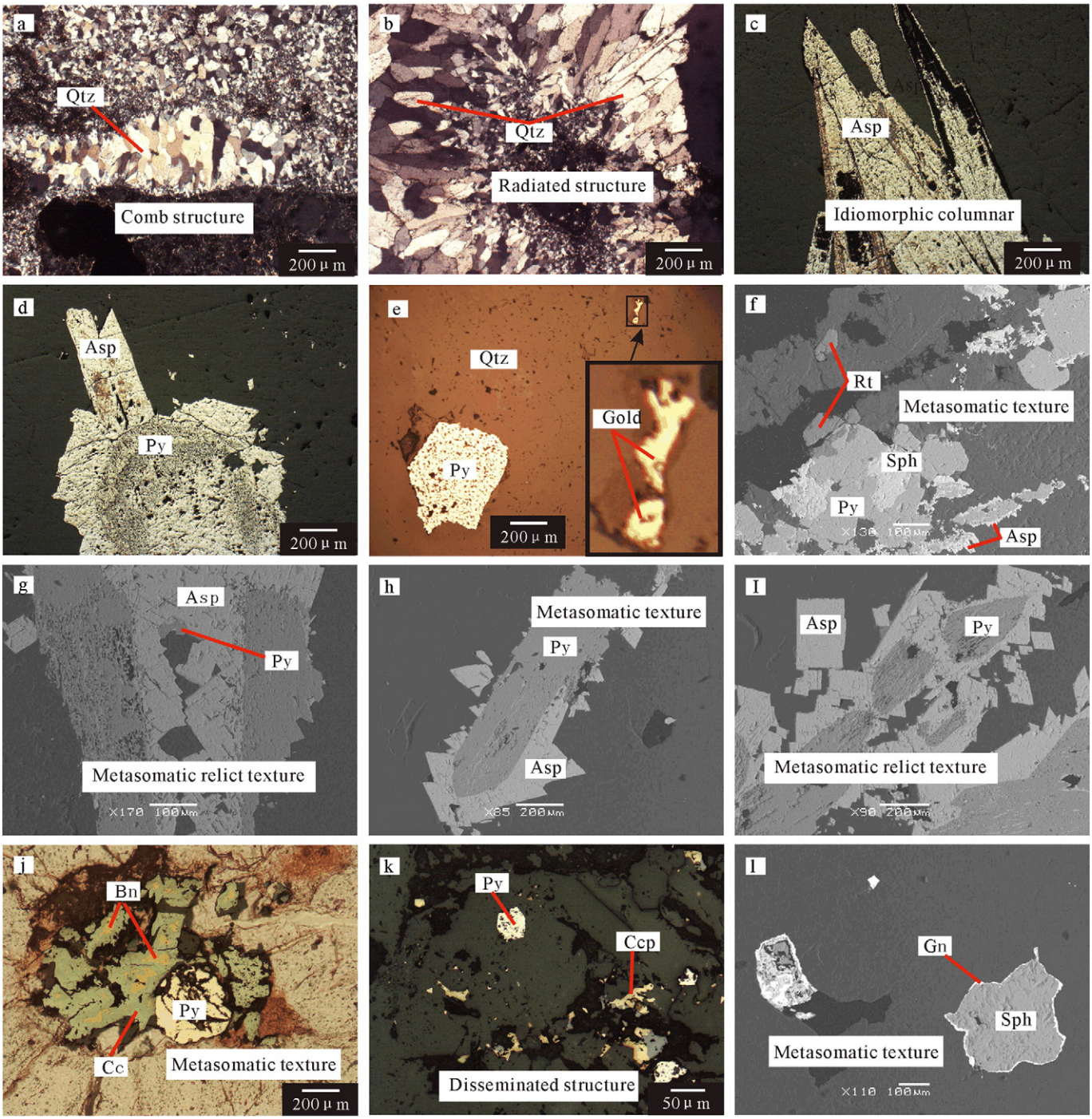

Fig. 4. Photographs of ore textures and structures from the Ciemas gold deposit. a: Comb quartz (cross-polarized light); b: Radiated structure, columnar quartz grew around the breccia (cross-polarized light); c: Idiomorphic columnar arsenopyrite; d: Metasomatic texture with pyrite replaced by columnar and granular arsenopyrite (reflected light); e: Metasomatic texture with pyrite and native gold; f: Metasomatic texture with pyrite replaced by arsenopyrite and sphalerite, rutile can be observed (back scattered electron image (BSE)); g: Metasomatic relict texture with xenomorphic pyrite wrapped with columnar arsenopyrite (BSE); h: Metasomatic texture with pyrite replaced by arsenopyrite within the crystal cracks (BSE); i: Metasomatic relict texture with xenomorphic pyrite wrapped by columnar arsenopyrite (BSE); j: Metasomatic texture with bornite replaced by chalcocite (reflected light); k: Disseminated chalcopyrite and granular pyrite within quartz; l: Metasomatic texture with sphalerite replaced by galena (BSE).

within the tectonic belt composed of andesite subjected to schistosity and fractures in the process of hydrothermal mineralization. Two periods of ore-formation have been identified: 1) The early phase characterized by altered andesite forming scattered pyrite on the surfaces of the schistosity and fractures without gold mineralization. 2) The second phase characterized by re-fragmentation of altered andesite, accompanied by ore-bearing hydrothermal filling metasomatism, forming fine vein–irregular net vein structures with gold mineralization. The ores are composed of siliceous cements, sulfide and precious metals. Alteration of the wall rocks mainly involves chloritization with silicification, limonitization, carbonatization and epidotization. The upper and lower rocks of the ore bodies are composed of clay minerals, and the thickness of the argillic zones is greater than 10 m. In addition, in the upper part of the ore body, several gold orebodies of carbonate vein–

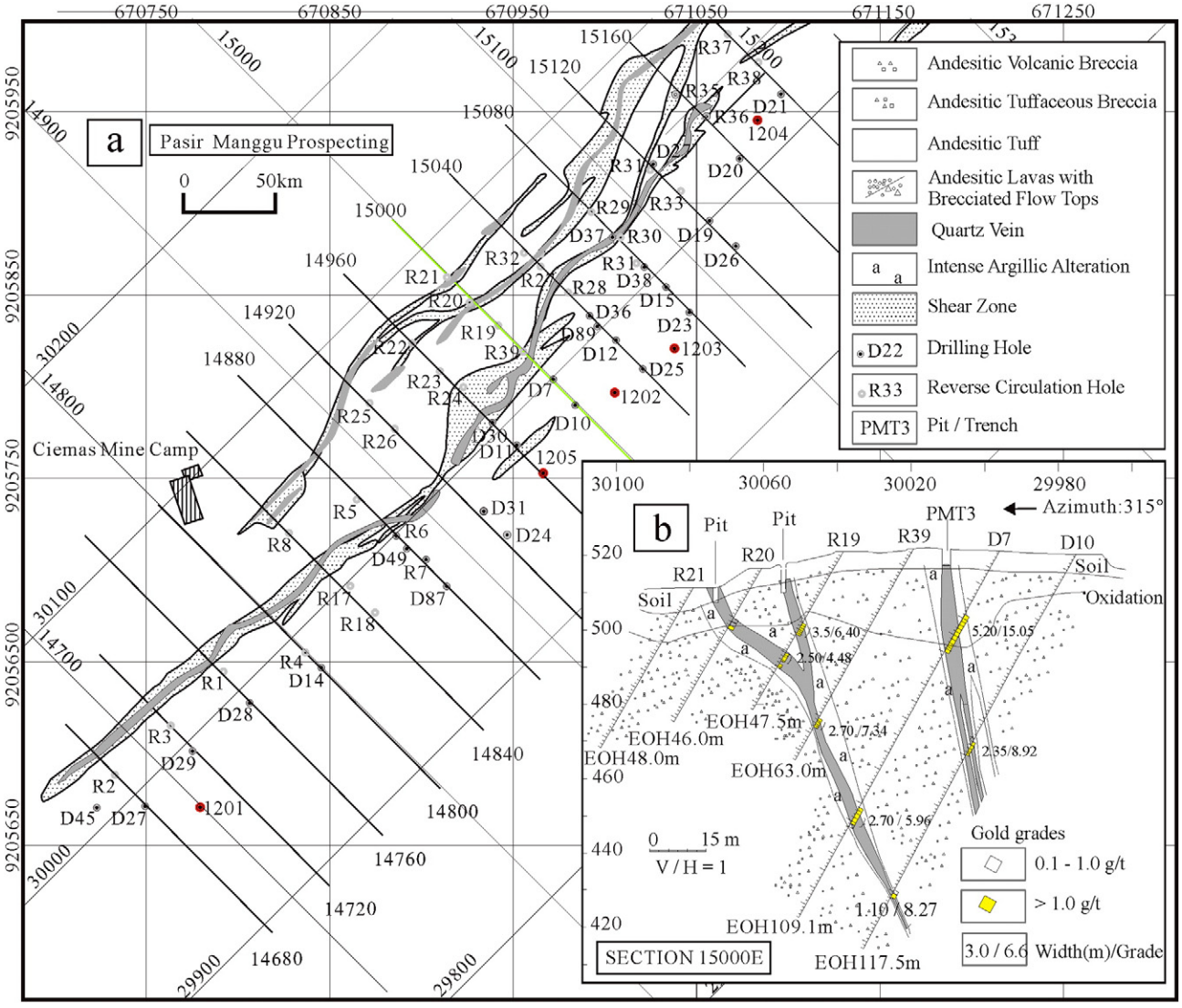

Fig. 5. Geological map of the Au deposit (a) and cross-section of the 15000E prospecting grid line (b) in Pasir Manggu (modified after Jonathan, 2007).

base metal veins are developed (Fig. 6b), and the metal minerals are mainly composed of sphalerite, pyrite and galena, in addition to associated gold and silver precious metal elements.

3.3. Porphyry ore deposits

In the Cipirit ore block, Ciemas dacite presents hypabyssal or ultra-shallow intrusion into the Jampang andesite Formation (Fig. 7a), intruded by late quartz diorite porphyrite (Fig. 7b). At the edge of the quartz diorite porphyrite, propylitization developed (Fig. 3a-1), forming oxidation zones 10 m to 100 m in width, with silicification and clay alteration on the surface (Fig. 3a).

As depicted in Fig. 7b, the drilling results indicate that the quartz diorite porphyrite (Fig. 3a-2) has pyrite and chalcopyrite mineralization but only with a lower Au content (<0.1 ppm). However, in the silicification, pyritization, and propylitization zone (limonitization zone, Fig. 3a-3, 4), the Au content is generally greater than 1 ppm. The morphology of ore body occurrence is varied, generally presenting a discontinuous layer and vein and crumb structure. Typically, a single ore body length is 20–80 m with a thickness of 3 to 10 m and a depth of 50 m. The average Au grade is 1.2 g/t. Outside of the propylitization zone, there are multiple parallel distributions of strong silicification and limonitization in the mesh quartz veins, accompanied with pyrite and galena, sphalerite, where the gold contents can range from 0.5 to 3 ppm. As the eight DDH (Diamond Drill Hole) borehole intervals in the mining area are more than 200 m, Jonathan (2007) estimated that the porphyry gold (Resources) amounts to 31.8 t, according to the surface engineering (Pit, Trench, Costean).

Metal minerals are mainly pyrite, chalcopyrite, arsenopyrite and magnetite, followed by magnetic pyrite, sphalerite, galena, a small amount of molybdenite, bornite, ilmenite, hematite and covellite. Gangue minerals are quartz, sericite, chlorite and calcite.

The ore exhibits in euhedral half-crystal, crystal, interstitial, and contain embedded textures. In addition, there are the skeletal textures of hydrothermal metasomatism, reaction-boundary textures, the textures of etching, residual textures, and pseudomorphism opacifying textures of solid solution separation. The main structures are block, vein and disseminated-net vein, and deformation and secondary changes to brecciated, colloidal, soil and honeycomb textures. The ore types are mainly oxidized, secondary sulfide and veinlet disseminated sulfide.

Minerals in the intrusion at the top of the propylitization are mainly composed of epidote, chlorite, albite and carbonate (calcite, dolomite

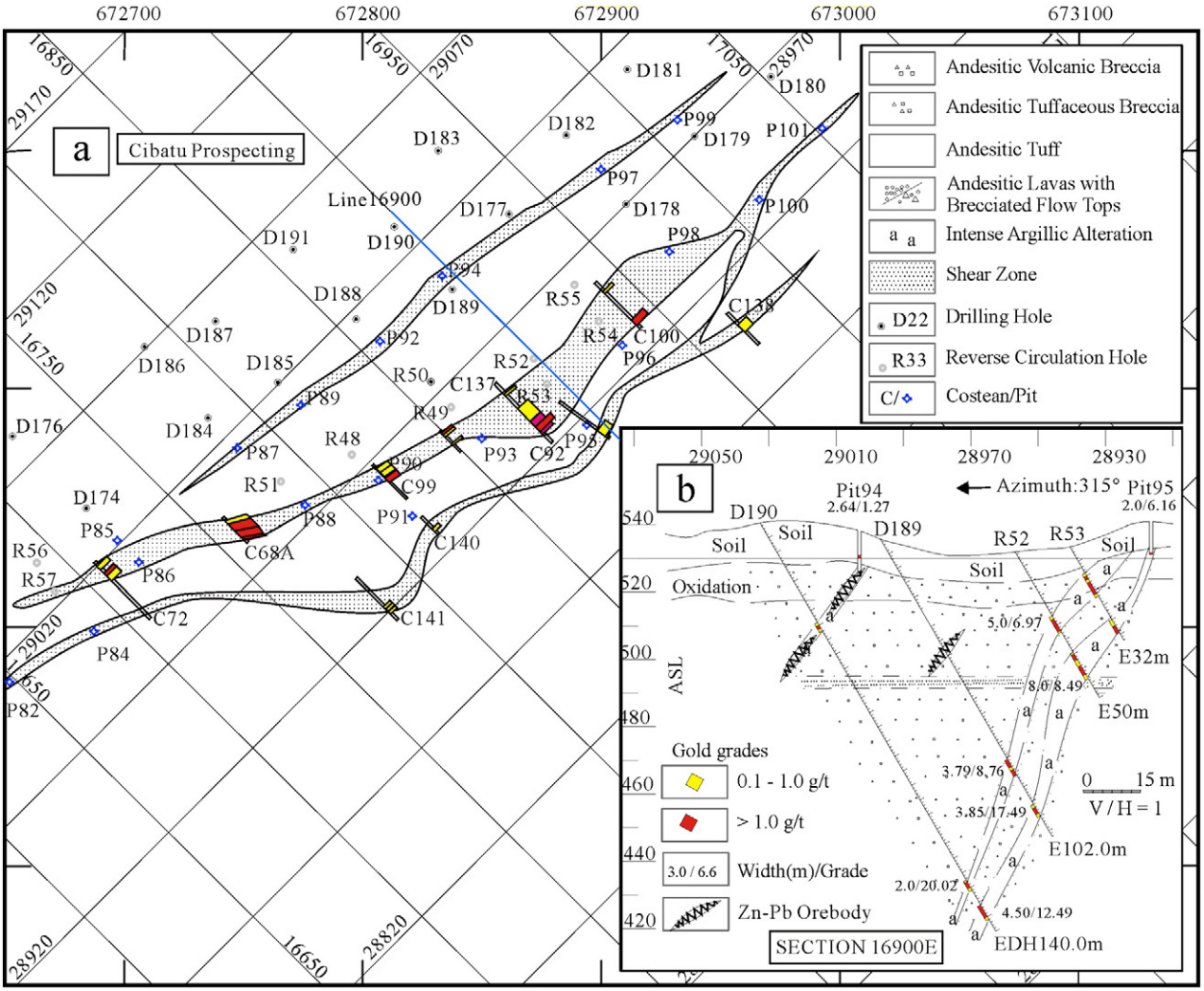

Fig. 6. Geological map of Au deposit (a) and cross-section of the 16900E prospecting grid line (b) in Cibatu (modified after Jonathan, 2007).

and ankerite), a small amount of sericite and magnetite, and pyrite. A clay zone is observed in the inner alteration belt, which is primarily composed of kaolinite and montmorillonite minerals.

4. Ore minerals and ore textures

The ore minerals are mainly pyrite, arsenopyrite, limonite, chalcopyrite, galena, sphalerite, bornite, chalcocite and rutile. The gangue minerals are mainly composed of quartz, plagioclase, chlorite, sericite, biotite, calcite, dolomite and ferrodolomite, among others (Fig. 4). Quartz is the main gangue mineral and displays a comb structure (Fig. 4a), radiated structure (Fig. 4b) and vein structure. The textures of ore include xenomorphic fine to micrograined granular, euhedral–subhedral granular, columnar, metasomatic and metasomatic relict. The ore structures are mainly disseminated, brecciated, comb, radiated, veinlet, interstitial sparse disseminated and massive.

A large amount of pyrite and arsenopyrite can be found in the ores. Pyrite mainly has a xenomorphic granular texture, and the arsenopyrite mainly has a columnar texture (Fig. 4c) and a euhedral–subhedral granular texture (Fig. 4d, h, i). Metasomatic texture is common in ores, such as arsenopyrite replaced pyrite (Fig. 4d, e, f, g, h, i), sphalerite replaced pyrite (Fig. 4f), chalcocite replaced bornite and galena replaced sphalerite (Fig. 4l). The pyrite was surrounded by the deuterogenic arsenopyrite and replaced by arsenopyrite within the crystal cracks. Some xenomorphic pyrite was wrapped in the columnar arsenopyrite and formed a metasomatic relict texture. Pyrite, arsenopyrite, limonite and chalcopyrite distributed in quartz display a disseminated structure (Fig. 4k).

5. Geochemistry

5.1. Sulfur isotope data

5.1.1. Sampling and analysis methods

In the Pasir Manggu ore block, three ore samples (P1, P2, and P3) were collected. In the Cipirit ore block, one ore sample was collected (CI). In the Cibak ore block, five ore samples were collected (C0, C04, C05, C09, and C14). In addition, three samples of andesite, quartz diorite porphyrite and amphibole tuff breccia were also collected (YN-1, YN-2 and YN-3, respectively). The sulfur isotopic data were analyzed at the State Key Laboratory of Environmental Geochemistry of Institute of Geochemistry, Chinese Academy of Sciences. A continuous flow isotope mass spectrometer, a CF-IRMS (EA–IsoPrime instruments), was used (method documented by Zhou et al., 2014). The measurement data are expressed using international standards for sulfur isotope CDT (Canyon Diablo Troilite) values and sulfur isotope standard GBW04414 (Ag_2S, $\delta^{34}S_{CDT} = -0.07 \pm 0.13‰$), GBW04415 ($Ag_2S$, $\delta^{34}S_{CDT} = 22.15 \pm 0.14‰$). The analysis errors are less than $\pm 0.2‰$ (2σ). The results are listed in Table 3.

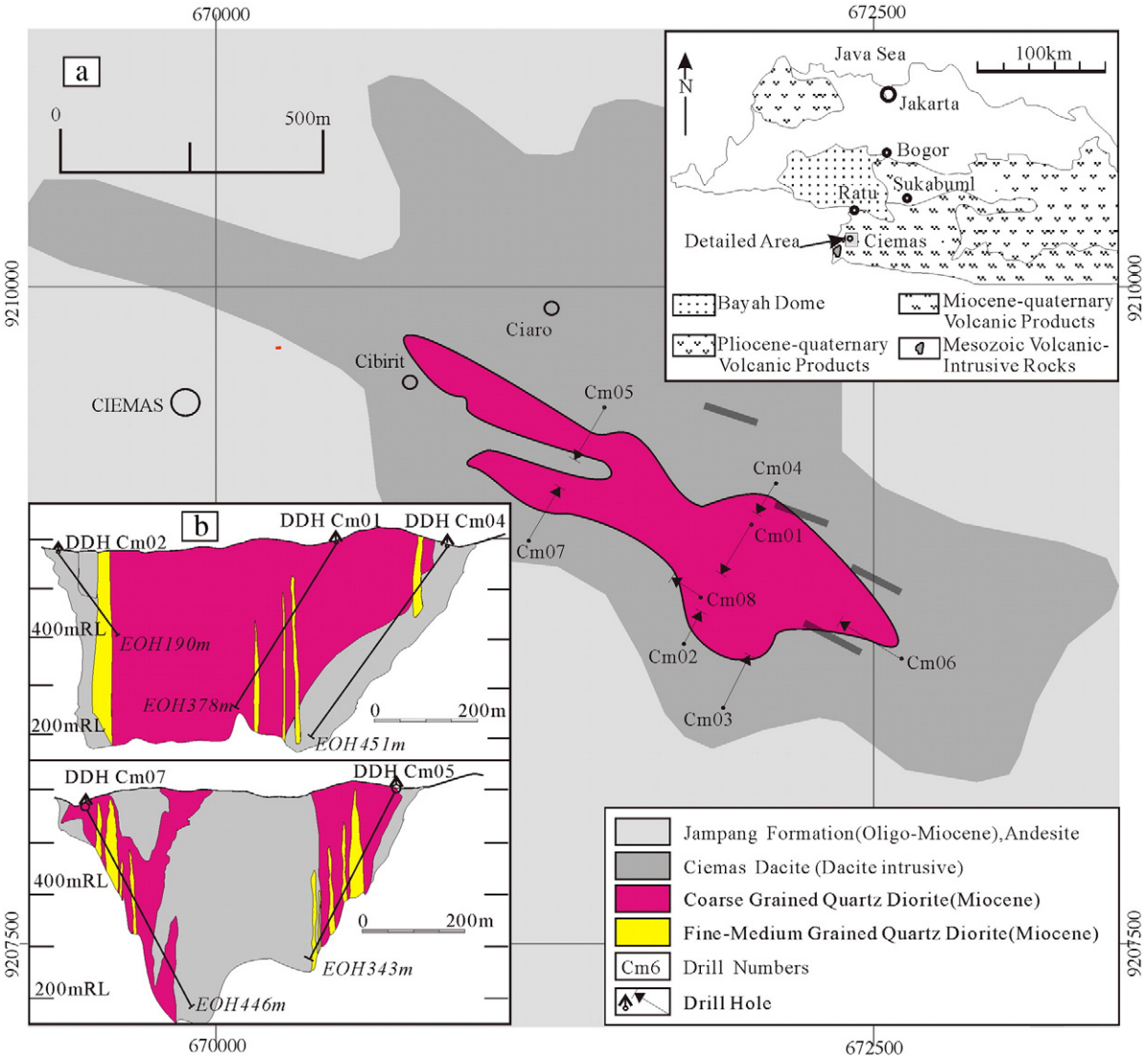

Fig. 7. Geological map of Au deposit (a) and cross-section of prospecting grid line (b) in Cipirit (modified after Jonathan, 2007).

5.1.2. Analysis results

Nine ore samples have $\delta^{34}S$ values ranging from 4.90‰ to 6.55‰, with a difference range of 1.65‰ and a mean of 5.54‰. Three rock samples have $\delta^{34}S$ values ranging from 3.71 to 3.85‰, with a difference range of 0.14‰ and a mean of 3.79‰ (Table 3). The sulfur compositions of the ore and rock samples are similar, suggesting that the sulfur sources are basically the same for each, being close to the characteristics of the mantle sulfur source. The wall rock samples are closer to the

Table 3
Sulfur composition and typical values of sulfide minerals from Ciemas gold deposit.

Ore body	Sample no.	Description of lithology	Mineral	$\delta^{34}S$ (‰)	$\pm 2\sigma$	Data sources
Pasir Manggu	P1	Ore bearing breccia	Pyrite	6.40	0.12	This study
Pasir Manggu	P2	Ore bearing breccia	Pyrite	6.55	0.10	
Pasir Manggu	P3	Altered andesite	Pyrite	5.68	0.01	
Cipirit	CI	Ore bearing quartzite	Pyrite	5.31	0.05	
Cibak	C0	Ore bearing quartzite	Pyrite	5.48	0.02	
Cibak	C04	Ore bearing quartzite	Pyrite	6.07	0.01	
Cibak	C05	Altered dacite	Pyrite	4.96	0.09	
Cibak	C09	Ore bearing quartzite	Pyrite	5.39	0.03	
Cibak	C14	Ore bearing breccia	Pyrite	4.90	0.07	
Cipirit	YN-1	Andesite	Pyrite	3.85	0.02	
Cipirit	YN-2	Quartz diorite porphyrite	Pyrite	3.81	0.01	
Cipirit	YN-3	Amphibolic tuff breccia	Pyrite	3.71	0.09	
Guntur	GU3.1	Lava flow	Total rock	4.5	Unknown	De et al. (2001a)
Guntur	GU5.1-I	Lava flow		3.4		
Guntur	GU5.1-II	Lava flow		3.2		
Krakatau	KR1	Volcanic cinder		4.1		

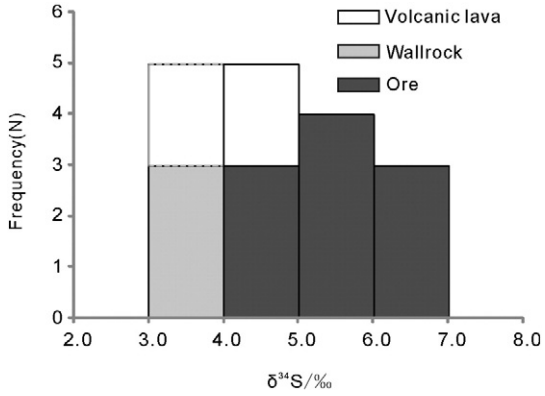

Fig. 8. Histogram of sulfur isotope of pyrite from the Ciemas gold deposit.

mantle source sulfur characteristics. On the statistical histogram (Fig. 8), three wall rock samples have $\delta^{34}S$ values similar to those of West Java Guntur lava flows and Krakatau volcanic slag (De et al., 2001a). The $\delta^{34}S$ values of nine ore samples are generally greater than those of the wall rock samples.

5.2. Zircon U–Pb isotope data

5.2.1. Samples and analysis methods

The sample collection includes quartz diorite porphyrite and its wall rocks of andesite and tuff breccia (samples CR-17 and CR-18 and CR-19, respectively). Zircons were separated using magnetic and heavy liquid separation methods and purified by handpicking under a binocular microscope. Approximately 100 zircon grains were mounted on an adhesive tape, enclosed in epoxy resin, polished, and then photographed under both transmitted and reflected light. The internal structures of the zircons were examined using the cathodoluminescence (CL) image technique. The U–Pb isotopic composition of zircons was analyzed with an Agilent 7700x ICP-MS coupled with a Resonetic Resolution 50-M ArF-Excimer laser source ($\lambda = 193$ nm) at the Institute of Geochemistry, Chinese Academy of Science. Zircon 91500 standard samples, the NISTSRM 91500, were used during analysis as controls (Hu et al., 2011; Liu et al., 2010a,b). The spot size of the ion beam was set to ~32 μm. The U–Pb ages of zircons were calculated by using the ISOPLOT program (Ludwig, 2003).

5.2.2. Analysis results

The three selected zircon samples have similar characteristics, including shallow color, a long cylindrical in shape and crystal length–width ratio of approximately 2:1 ~ 5:1. The zircons have good euhedral shapes with a completed cylinder and cone. Cathodoluminescence (CL) images show that the zircons have shock rings with a distinctive igneous origin (Fig. 9).

In the $^{206}Pb/^{238}U$–$^{207}Pb/^{235}U$ age concordia diagram (Fig. 10), the analyzed data points fall near the concordia. Zircon $^{207}Pb/^{235}U$ age changes are greater, and the $^{206}Pb/^{238}U$ ages are relatively concentrated. The calculated zircon $^{206}Pb/^{238}U$ weighted average ages are 17.1 ± 0.4 Ma (MSWD = 3.8, n = 15) (amphibole quartz porphyry, Fig. 10a), 17.1 ± 0.4 Ma (MSWD = 3.7, n = 25) (tuff breccia, Fig. 10b) and 17.5 ± 0.3 Ma (MSWD = 3.3, n = 27) (andesite, Fig. 10c). The ages for the determination of the three samples are close to each other, within analysis error, indicating that in this study area, the andesite

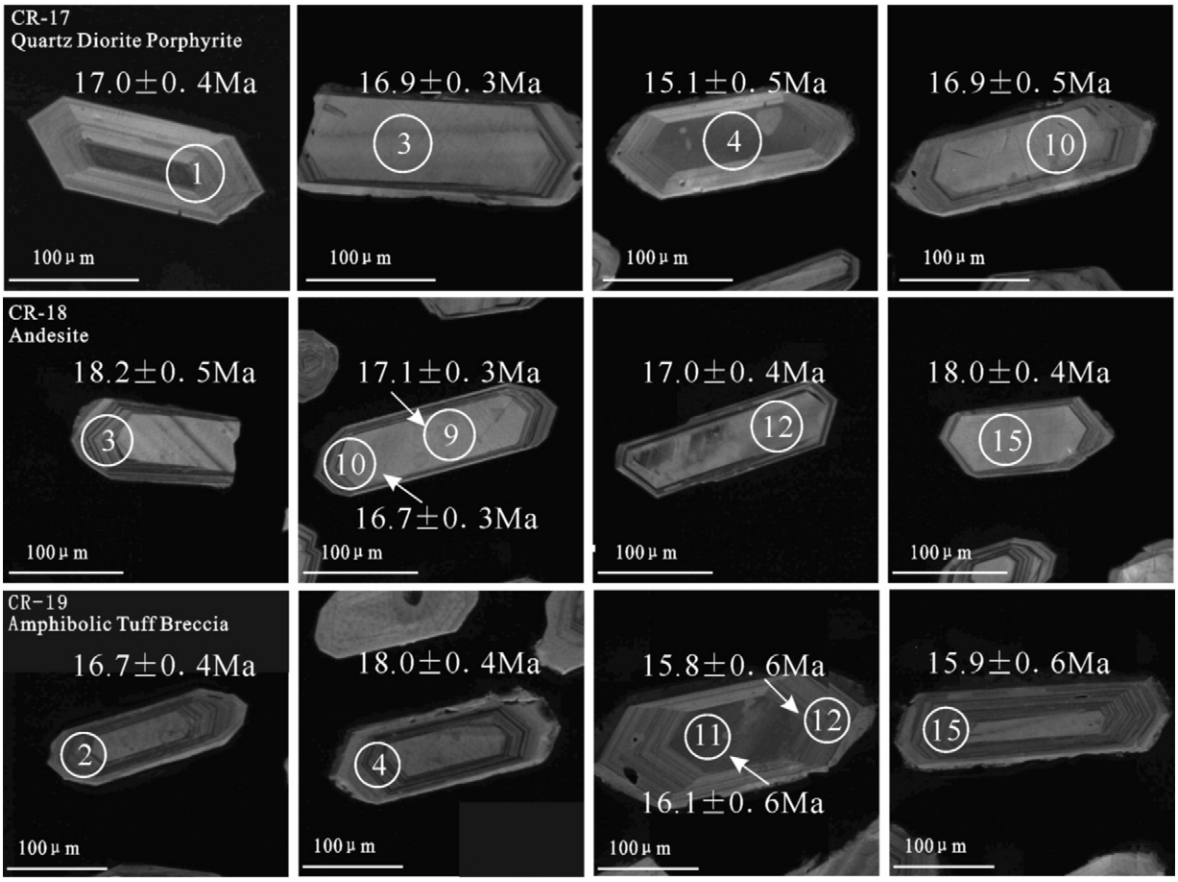

Fig. 9. CL images of representative zircons analyzed for in situ U–Pb of quartz diorite porphyrite, andesite and amphibolic tuff breccia in Ciemas.

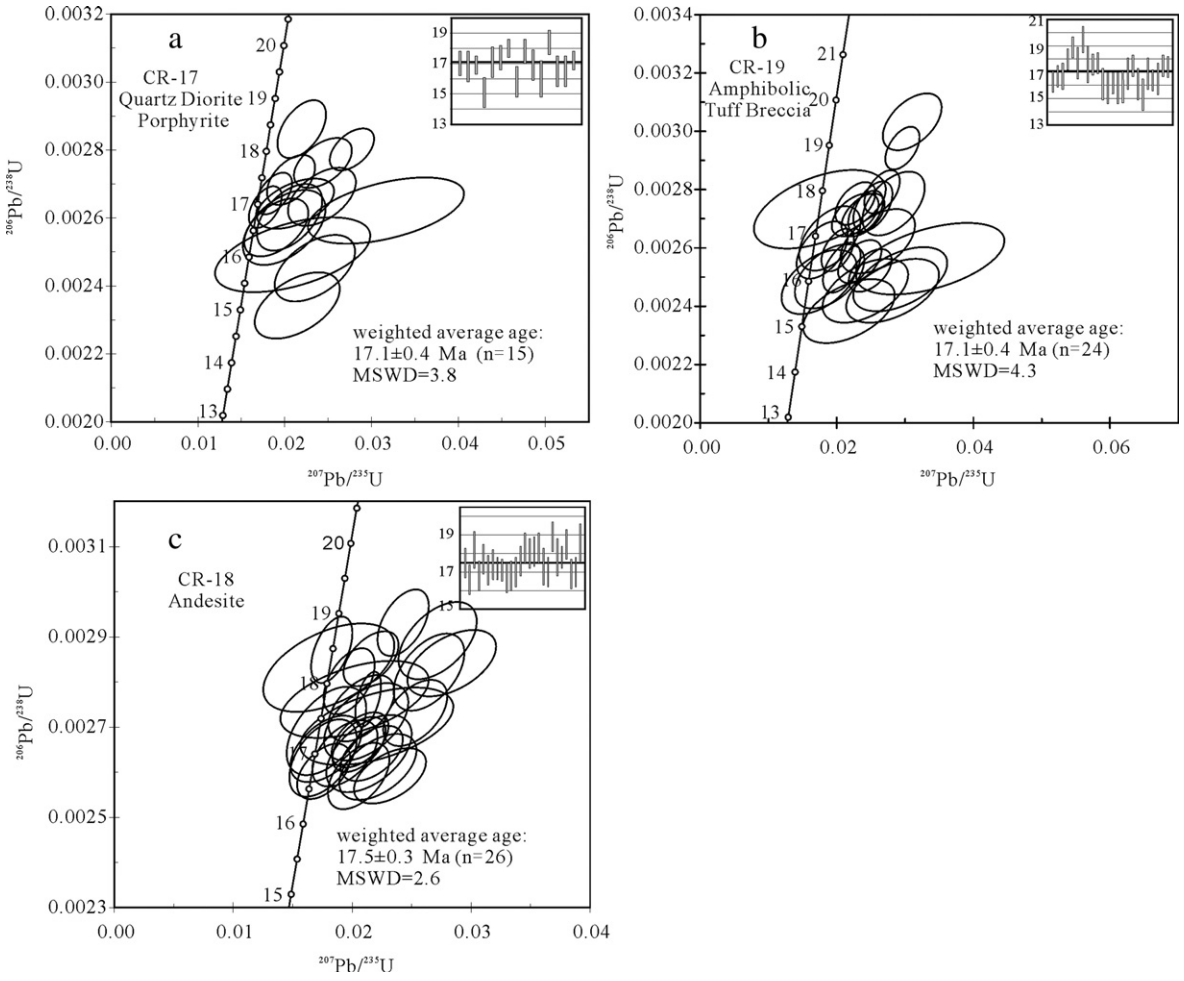

Fig. 10. Zircon U–Pb concordia diagram of quartz diorite porphyrite (a), amphibolic tuff breccia (b), and andesite (c) in Ciemas.

eruption was within a short period in the early Miocene, followed by a magma intrusion.

5.3. Major and trace elements

The sampling and analytical methods are as follows: In the Pasir Manggu ore block, five samples were collected (PSR-2, PSR-1–3, PSR-4, and PSR-E-1). In the Sekolah ore block, three samples were collected (SKL-1, SKL-2, and SKL-3). In the Cigombong ore block, two samples were collected (CGB-1 and CGB-2), and in Cipirit ore block, two samples were collected (CPT-1 and CPT-2).

The major elements and trace elements (including rare earth elements) were analyzed in the ALS Laboratory Group, an Australian ICP-MS analytical lab in Guangzhou.

For major element analysis, a calcined or ignited sample (~0.9 g) was added to lithium borate flux (~9.0 g, 50% $Li_2B_4O_7$–$LiBO_2$), mixed well and fused in an auto fluxer at a temperature between 1050 and 1100 °C and then cooled to form a flat molten glass disk, which was then analyzed by ME-XRF-06, with analytical precisions as follows: SiO_2, 0.8%; Al_2O_3, 0.5%; Fe_2O_3, 0.4%; MgO, 0.4%; CaO, 0.6%; Na_2O, 0.3%; K_2O, 0.4%; MnO, 0.7%; TiO_2, 0.9%; and P_2O_5, 0.8%. The analytical uncertainties were less than 1%.

Trace elements were analyzed by inductively coupled plasma-mass spectrometry (ICP-MS) of ME-MS81. We used the HNO_3 + HF seal dissolution method for trace elements and REE determination by adding the Rh internal standard and transferring the sample solutions into a 1% HNO_3 medium. The analytical precisions of trace elements were as follows: Ba, 2.7%; Ta, 2.1%; Nb, 1.6%; Zr, 2.2%; Hf, 2.1%; Th, 2.1%; U, 3.4%; Pb, 3.2%; Ga, 1.9%; Cr, 5.3%; Co, 0.8%; Ni, 11%; Cu, 3.5%; Rb, 2.1%; Sr, 1.7%; Sc, 4.2%; V, 3.2%; and Zn, 3.0%.

Rare earth elements were analyzed by cation exchange separation-inductively coupled plasma atomic emission spectrometry (ICP-AES) with the following analytical precision: La, 4.7%; Ce, 5.2%; Pr, 1.8%; Sm, 4.7%; Eu, 1.2%; Gd, 1.4%; Tb, 3.2%; Dy, 4.3%; Ho, 2.4%; Er, 3.9%; Tm, 4.8%; Yb, 4.3%; Lu, 3.9%; and Y, 1.8%.

Analysis results: Among the 12 ore samples, we chose seven strong pyritization samples to determine the Co/Ni ratio of projection (Fig. 11a). Most of the samples plotted in the origin of the hydrothermal type deposit area. The metallogenic elements (Au and Cu, As, and other trace elements) display some positive correlations between Au and Cu elements (Fig. 11b), and incompatible elements Cr, Ni, Co and V display a negative correlation (Fig. 11c, d). Au and incompatible elements, on the whole, display a negative correlation (Table 4). However, Au has poor correlation with the large ion lithophile elements K, Sr and Ba (Fig. 11e). For the minerals, a diagram of trace elements relative to the standardization of the primitive mantle (Palme and O'Neill, 2003) is shown in Fig. 12. For the incompatible element Cr to high-field strength elements P, there is loss then slight enrichment with a gradual growth. Nearly all of the trace element contents are near the Earth's crustal content (Palme and O'Neill, 2003), and the incompatible elements Cr, Ni, Co and V have similar variations.

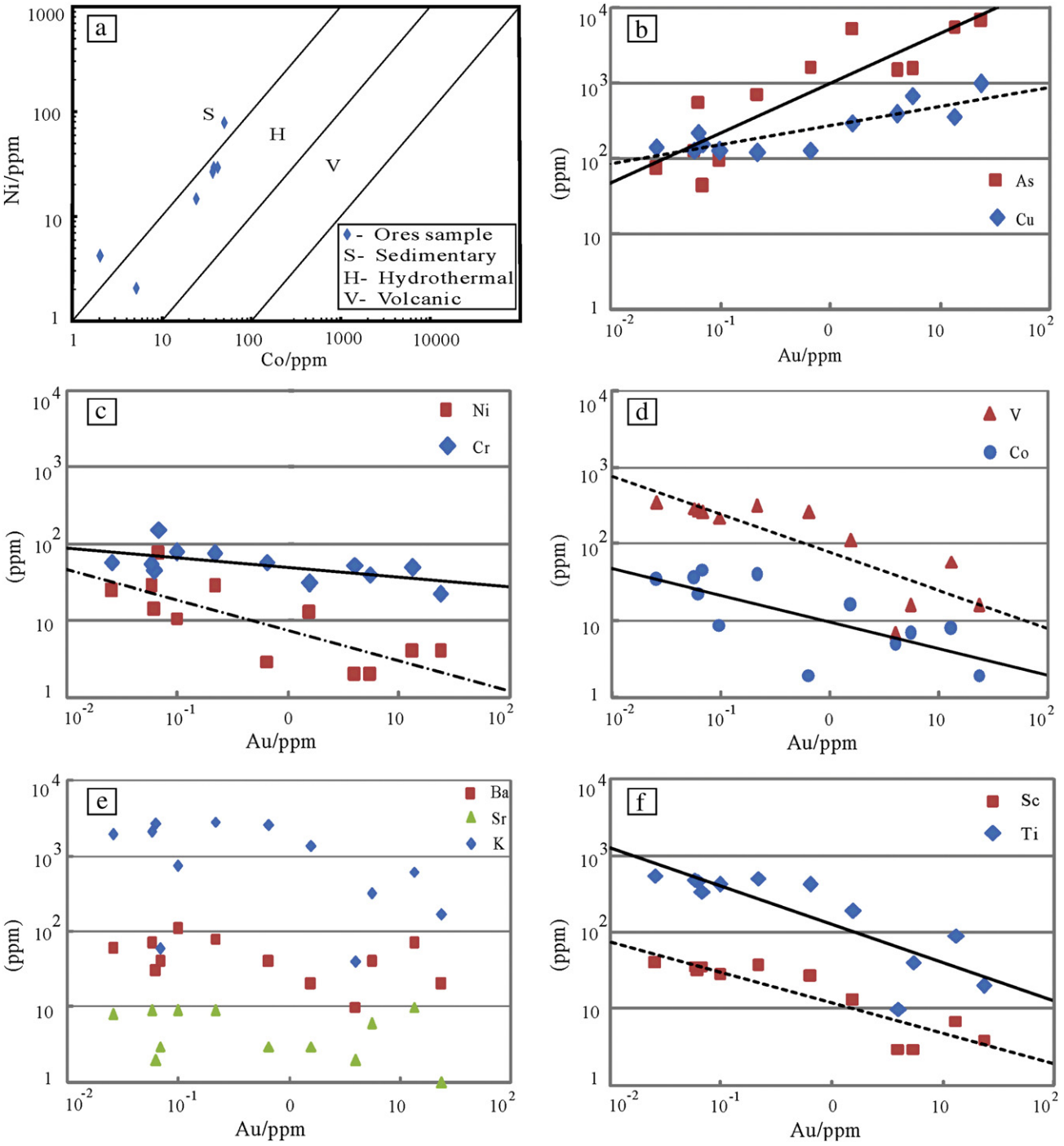

Fig. 11. Diagram showing the correlations between gold and trace elements.

6. Fluid inclusions

6.1. Sample and analysis method

Quartz ore samples were taken from Pasir Manggu (sample labels P1 and P2), Cipirit (CI) and Cibak (sample labels C0, C04, C05, C09, and C14) of each gold ore block (Fig. 1, Table 5). Fluid inclusion testing work was conducted at the State Key Laboratory of Ore Deposit Geochemistry of Institute of Geochemistry, Chinese Academy of Sciences. Using a Linkam THMSG type 600 stage, the technical parameters were as follows: platinum resistance sensor, temperature measurement range −196 °C–600 °C, and freezing and heating data accuracy of ±0.1 °C and ±2 °C, respectively. Measurements of the freezing point and the formula of freezing point drop in temperature and salinity of aqueous inclusions salinity were performed according to Bodnar (1993). Using the inclusion calculation software MacFlincor (Brown, 1989) under a NaCl–H_2O system, we selected the Brown and Lamb (1989) formula to calculate the fluid density. The pressure values of ore-forming fluids were calculated by the homogenization temperatures and salinities of fluid inclusions (Liu and Duan, 1987). The statistical histogram and scatter diagram of the fluid inclusion data were processed using Geokit software (Lu, 2004).

Table 4
Trace elements compositions of the ore from the Ciemas gold deposit.

Ore body	Sample no.	Description of lithology	Cr/ppm	Ni/ppm	Co/ppm	V/ppm	K/%	Sr/ppm	Ba/ppm	La/ppm	Ti/%	Sc/ppm	P/ppm	Au/ppm	Cu/ppm	As/ppm
Pasir Manggu	PSR-1	Altered quartzite	58	3	2	262	2.56	3	40	10	0.42	27	200	0.652	127	1640
Pasir Manggu	PSR-2	Altered tuff breccia	31	13	16	111	1.34	3	20	8	0.19	13	40	1.58	293	5290
Pasir Manggu	PSR-3	Altered quartzite	45	14	23	273	2.71	2	30	6	0.46	31	50	0.063	220	561
Pasir Manggu	PSR-4	Limonited quartzite	49	4	8	59	0.62	10	70	7	0.09	7	70	13.35	350	5550
Sekolah	SKL-1	Pyritized quartzite	74	28	40	316	2.84	9	80	8	0.5	37	640	0.217	119	709
Sekolah	SKL-2	Pyritized breccia	54	28	36	297	2.12	9	70	10	0.48	36	710	0.058	128	129
Sekolah	SKL-3	Pyritized andesite	58	25	35	350	1.92	8	60	6	0.55	40	740	0.026	140	74
Pasir Manggu	PSR-E-1	Pyritized quartzite	23	4	2	16	0.17	1	20	9	0.02	4	70	23.6	969	6680
Cigombong	CGB-1	Pyritized quartzite	52	2	5	7	0.04	2	10	8	0.01	3	450	4.02	382	1470
Cigombong	CGB-2	Pyritized quartzite	40	2	7	16	0.32	6	40	7	0.04	3	110	5.53	672	1530
Cipirit	CPT-1	Pyritized dacite	153	74	47	259	0.06	3	40	40	0.34	36	50	0.069	155	42
Cipirit	CPT-2	Limonited dacite	78	11	9	222	0.74	9	110	10	0.42	28	280	0.099	124	94

6.2. Results

6.2.1. Types of fluid inclusions

This experiment examined a total of eight inclusion samples (Figs. 13 and 14). The types of fluid inclusions in quartz are relatively simple; according to the inclusion phase at room temperature, they can be divided into two phases: gas–liquid inclusions and pure liquid inclusions. Gas liquid phase inclusions account for the vast majority, with a lack of CO_2-containing inclusions and mineral-containing inclusions. Gas liquid phase inclusions are rich in liquids, and their liquid filling degree is between 70% and 85%. No boiling inclusion was observed. Inclusion linear distributions do not cut though the quartz crystal, which suggests that the inclusions are native and secondary inclusions. Most single inclusions are in an irregular shape with a diameter of less than 15 μm.

6.2.2. Homogenization temperature

In the Pasir Manggu ore block, we measured 35 homogenization temperatures, most of which were concentrated in the 240–320 °C temperature range, with an average of 290.7 °C (Table 5). In the Cipirit ore block, we measured 33 inclusion homogenization temperatures, most of which were concentrated in the 260 to 320 °C, with an average of 289.2 °C. In the Cibak ore block, we measured 101 homogenization temperatures, varying from 146.8 to 447.0 °C, with a peak temperature between 280 and 320 °C and an average of 289.3 °C, close to the above two ore blocks. Statistical results indicate that the 169 homogenization temperatures change between 146.8 and 447.0 °C with a peak temperature between 240 and 320 °C and an average of 290.4 °C, and the histogram is in a single peak (Fig. 14a). Generally, these inclusions belong to the low-temperature group and occasionally to middle–high temperature group, displaying the magmatic-derived hydrothermal fluid system.

6.2.3. Salinity

In the Pasir Manggu ore block, we measured the freezing point temperature range from −13.5 to −10.9 °C. The corresponding salinity (wt.% NaCl) is from 17.34 to 14.87, and the salinity values in each interval are more uniform and mostly concentrated in the range of 16.35 to 15.25 (Table 5). In the Cipirit ore block, we measured the freezing point temperature range from −14.0 to −10.9 °C. The corresponding salinity (wt.% NaCl) is from 17.79 to 14.87, and the salinity is concentrated in the 14.86–15.28 range. In the Cibak ore block, we measured the freezing point temperature and found a range of −13.9 to −7.2 °C, corresponding to a salinity (wt.% NaCl) range from 17.70 to 10.73. The salinity range is greater for the Cibak block. A larger proportion is concentrated in the 13.71–16.71 range. In these three ore blocks, we found that inclusion salinity (wt.% NaCl) ranges from 10.73 to 17.79 and is mainly concentrated in the 14.75 to 16.75 range (Fig. 14c), indicating low salinity. A homogenization temperature–salinity scatter plot (Fig. 13d) showed that the inclusion salinity values increased with temperature increases; i.e., the high-temperature fluid had high salinity.

6.2.4. Fluid density, pressure and estimation of metallogenic depth

Analysis of a total of 101 quartz inclusions with fluid density values was performed. Among these inclusions, 21 density values of the Pasir Manggu ore block range from 0.874 to 0.961 g/cm^3; 11 density values of the Cipirit ore block range from 0.897 to 0.947 g/cm^3; 69 fluid density values of the Cibak ore block range from 0.646 to 0.999 g/cm^3. Among these values, 11 of the measured fluid density values are less than 0.850 g/cm^3. In general, three of the ore blocks' fluid density values are concentrated in the range of 0.850 to 0.950 g/cm^3 (Table 5), and only the Cibak ore block samples appear to have low fluid density values (Fig. 14b). Ore-forming fluid pressure values in the Pasir Manggu ore block are between 9.0 and 32.6 MPa. The Cipirit ore block values are between 5.0 and 19.5 MPa, and the Cibak ore block values are between 4.1

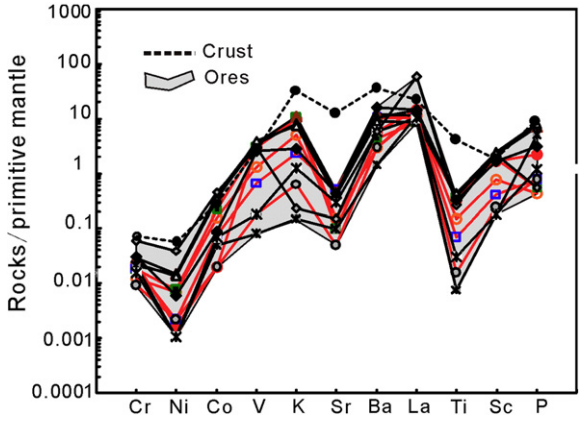

Fig. 12. Diagram showing the pattern of primitive mantle-normalized trace elements (primitive mantle data from Palme and O'Neill, 2003).

and 46.8 MPa. Supposing a 27 MPa/km pressurization rate (Xu et al., 2012), the formation depth of the three ore blocks range from 330 to 1210 m, 180 to 640 m, and 150 to 1730 m, respectively, indicating a hypabyssal formation environment.

7. Discussion

7.1. Deposit features indicate three different types of mineralization

According to their ore textures and geological characteristics, the mineralization can be broadly divided into three types.

1) The first are fault-controlled ore bodies, occurring in schist-like tectonite, cataclastic rock and argillic belts (Cibatu, Cikadu and Sekolah). Due to tectonic alteration, a granular blastic texture was formed, as were a cataclastic structure, a block structure and a schistose structure. Pyrite is often observed on the structural surface along the cataclastic rock interface or mylonite with scatted distribution. The ore minerals are mainly pyrite, quartz, arsenopyrite and sphalerite. Wall rock alteration is common with chloritization, sericitization, carbonatization and argillic alteration (illite and montmorillonite), and the development of carbonate-based metal mineralization on the tops and bottoms of ore bodies (Fig. 7b). The mineralization features are similar to the typical low sulfide content formed by fluid-mixing type gold deposits (Corbett, 2002). The Acupan and Kelian deposits near a hypabyssal intrusive body are typical examples of low-sulfide gold deposits along a fracture structure (Cooke and McPhail, 2001; Davies et al., 2003; Heinrich, 2005).
2) The second type is the quartz–sulfide vein ore body (Pasir Manggu, Cigombong, Cileuweung and Cibak). The ore body occurrence can be further divided into massive quartz veins, open growth quartz veins, multiple quartz vein zones and stockwork quartz veins (Fig. 15). The ore mineral components include quartz, pyrite, arsenopyrite and arsenic sulfide copper ore. Wall rock alteration is strongly argillic (mainly kaolinite, illite and montmorillonite). These characteristics are similar to a typical high-sulfide type gold deposit (Carrillor et al., 2003; Corbett, 2002).
3) The third type is porphyry (Cipirit). Part of the mineralization occurred in the quartz diorite porphyrite (Fig. 3a-2). There are pyrite and chalcopyrite, but the gold content is less than 0.1 ppm. The majority of the ore body develops in the propylitization zone, and the ore mineral assemblage is composed of pyrite, chalcopyrite, magnetite and arsenopyrite. Wall rock alteration mainly involves epidotization, chloritization, albitization and carbonatization. A moderate argillic alteration occurs inside the alteration zone, mainly with kaolinite and montmorillonite.

These three types of ore bodies are within the same field (Fig. 2), and their occurrence in space is near the contact zone and intrusion fractures. The genesis belongs to a continuous metallogenic series. There are cases of a variety of causes with internal relationships to ore deposit types in the same mining area, such as the Kelly Au–Ag deposit of mineral assemblage, showing the hydrothermal system evolution from low-sulfur, medium-sulfur and high-sulfur (Deyell et al., 2003). Lepanto high-sulfide-type Cu–Au deposits from the far southeast of this region also occur in porphyry copper (Hedenquist et al., 1998).

7.2. Three different mineralization types have the same source of ore-forming materials

Java is part of the Sunda arc belt, which formed a series of calc-alkaline magmatic rocks since the Eocene (Bemmelen, 1949, 1970; Katili, 1975; Nicholls et al., 1980; Whitford et al., 1979). The ages of these volcanic rocks have been determined using the K–Ar method (Soeria et al., 1994). Three periods of volcanic activity are proposed from the south to the north, i.e., the south part belongs to the late Eocene to early Miocene (40–18 Ma). The central part belongs to the late Miocene to Pliocene (12–2 Ma), and the north part belongs to the Quaternary (Fig. 1b). The Ciemas gold deposit is located in an active volcanic zone in southern Java, and the mining area exposes quartz diorite porphyrite, andesite and amphibolic tuff breccia. The zircon U–Pb ages represent the intrusion and eruptive magma crystallization periods (Table 1), and their ages are very close to each other within the error ranges (Fig. 10), demonstrating that they belong to late Eocene to early Miocene igneous activities.

The $\delta^{34}S$ values of the wall rocks range from +3.71 to +3.85‰, similar to those of the West Java Guntur lava flows and Krakatau volcanoes (De et al., 2001a), which are considered to have a mantle magma source mixed with continental basement sediments (De et al., 2001b). Based on this isotopic geochemistry and geochronological work, we propose that the Indian Plate subducted beneath the Eurasian Plate, and the sediments with enriched ^{34}S were mixed with mantle magmatic melt in the

Table 5
Formation temperature of the fluid inclusions within quartz from Ciemas gold deposit.

Sample no.	Determine quantity	Grain (μm)	Liquid-vapor ratio (%)	Th (°C) Range mean value (quantity)		Tm (°C)	Salinity (wt.% NaCl) Range mean value (quantity)		Density (g/cm^3)	Pressure (Mpa)	Ore types
P1	18	3 ~ 41	80 ~ 96	230.8 ~ 313.4	279.4 (18)	−13.5 ~ −11.5	15.47 ~ 17.34	16.32 (12)	0.874 ~ 0.961	12.2 ~ 21.0	Ore bearing breccia
P2	17	3 ~ 43	76 ~ 92	285.4 ~ 350.8	303.3 (16)	−13.5 ~ −10.9	14.87 ~ 17.34	15.87 (10)	0.876 ~ 0.914	9.0 ~ 32.6	Ore bearing breccia
CI	33	4 ~ 33	76 ~ 96	237.8 ~ 332.5	289.2 (32)	−14.0 ~ −10.9	14.87 ~ 17.79	16.13 (11)	0.897 ~ 0.947	5.0 ~ 19.5	Limonited quartzite
C0	20	4 ~ 36	78 ~ 95	194.0 ~ 354.0	281.6 (23)	−11.4 ~ −7.2	10.73 ~ 15.37	12.95 (17)	0.792 ~ 0.985	12.1 ~ 46.8	Pyritized quartzite
C04	18	3 ~ 35	85 ~ 97	146.8 ~ 411.0	264.1 (19)	−12.7 ~ −7.3	10.86 ~ 16.62	13.78 (13)	0.646 ~ 0.999	4.1 ~ 28.1	Pyritized quartzite
C05	22	3 ~ 28	75 ~ 93	256.5 ~ 431.7	304.2 (20)	−13.9 ~ −11.5	15.47 ~ 17.70	16.26 (14)	0.702 ~ 0.934	19.6 ~ 33.1	Pyritized quartzite
C09	19	4 ~ 28	60 ~ 97	168.0 ~ 447.0	299.6 (24)	−13.0 ~ −8.9	12.73 ~ 16.89	14.96 (15)	0.676 ~ 0.972	2.3 ~ 28.0	Altered dacite
C14	22	3 ~ 28	80 ~ 96	247.0 ~ 346.7	294.9 (17)	−12.2 ~ −10.4	14.36 ~ 16.15	15.23 (10)	0.859 ~ 0.935	4.1 ~ 35.1	Pyritized quartzite

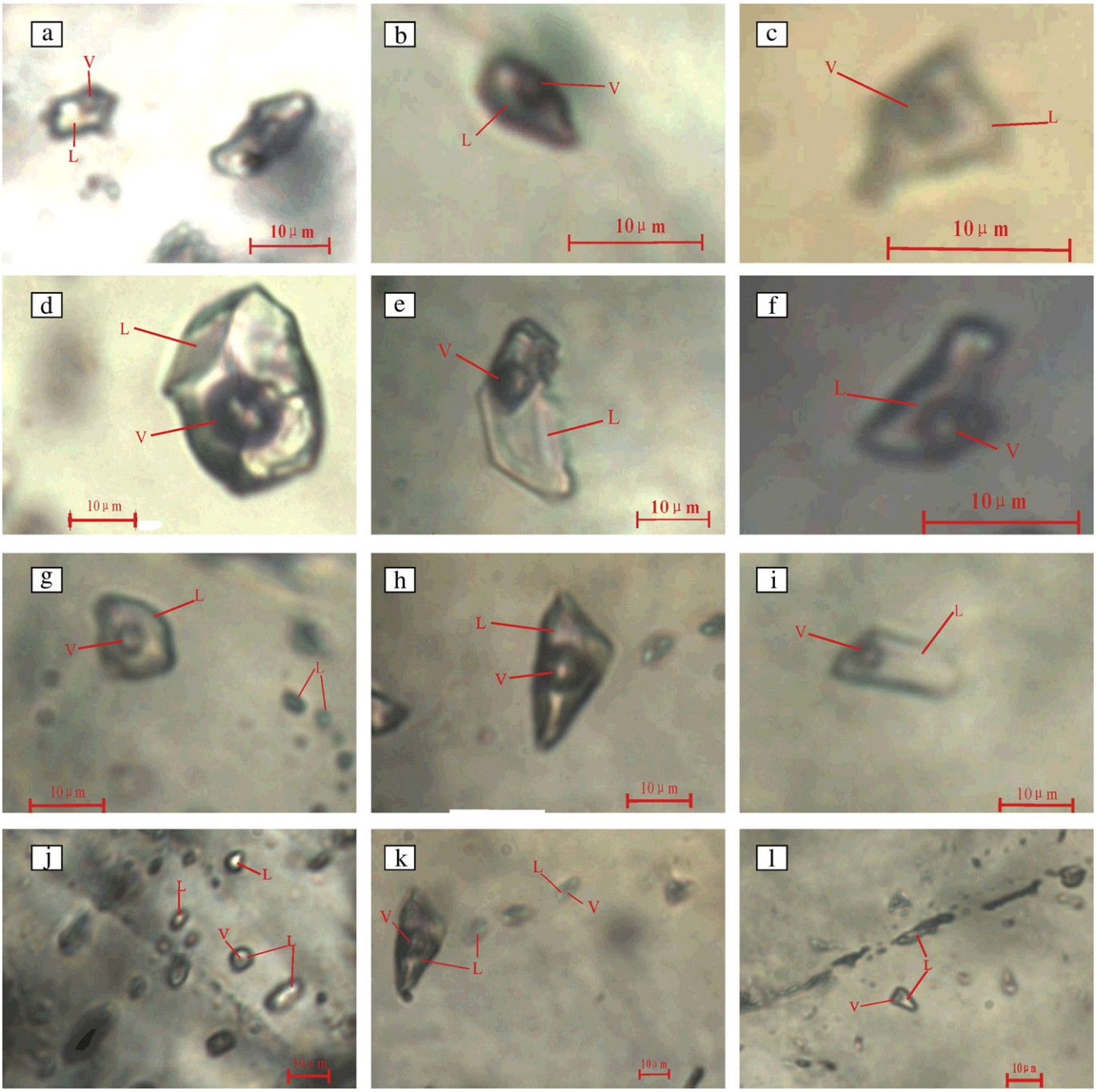

Fig. 13. Microscope photographs of fluid inclusions within quartz from Pasir Manggu (a to c), Cibak (d to f), and Cileuweung (g to l). a — small crystal from inclusion (left), from P1; b — small regular inclusion, from P2; c — irregular inclusion (L > 90), from P2; d — incomplete crystal inclusion, from CI; e — large irregular inclusion, appears trapezoidal, from CI; f — small irregular inclusion, from CI; g — beating inclusion under normal temperature, from C05; h — triangular inclusion, from C09; i — liquid-rich gas–liquid two-phase inclusion, from C04; j — complete liquid phase inclusion, from C09; k — inclusions group with significant size difference, from C04; l — linearly distributed inclusions, from C05.

arc region. Consequently, subduction led to a large oblique fault zone and forced the magma migration upward. Relative to the wall rocks, the $\delta^{34}S$ values of ores are more enriched (average $\delta^{34}S = +5.54‰$), suggesting that ore materials were derived from magma transporting ore-forming fluids in the process of migration; thus, the enriched ^{34}S may be incorporated into the ore-forming system. The sulfur isotopic compositions of the different ore bodies of the mines are consistent, indicating that they have the same material source (Fig. 8).

According to trace element features of the different types of ores, the incompatible elements (Cr, Ni, Co, V) trends are nearly consistent, whereas high-field-strength elements (La, Ti, Sc and P) change greatly, also indicating that the ore materials have the same source (Fig. 12). Large ion lithophile elements (K, Sr) fluctuate between weak depletion, weak enrichment and enrichment of Ba (less than the level of the Earth's crust), which may indicate that the fluid was not only derived from magmatic fluid but also may be derived from sea water.

7.3. Fluid inclusions reflecting high-sulfur hypabyssal characteristics of a low temperature hydrothermal deposit

In the study area, fluid inclusions in the quartz-vein type sulfide ore body have gas–liquid phase inclusions with rich liquids and a lack of CO_2

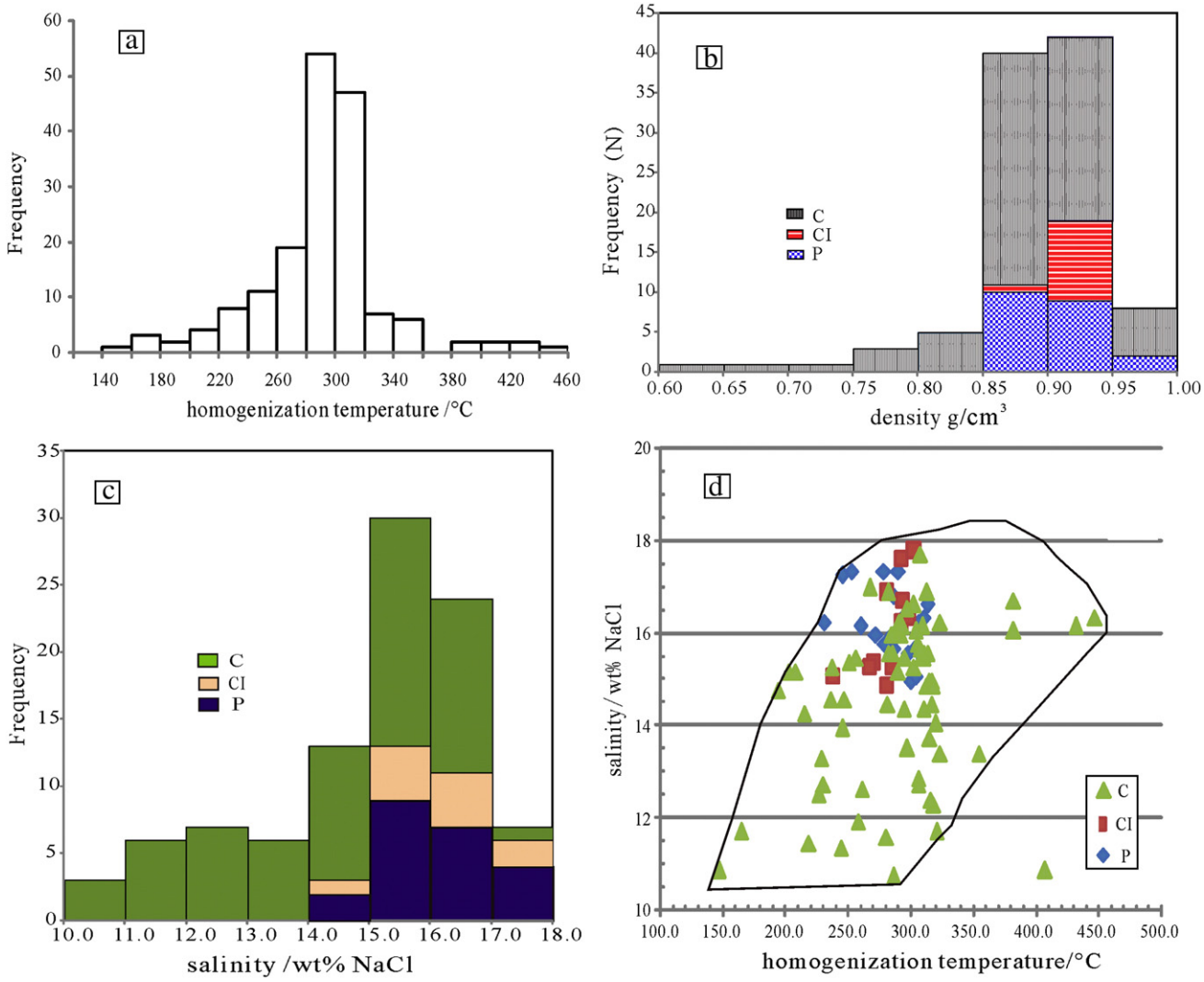

Fig. 14. Diagram showing the relationship between homogenization temperature, salinity and density of the fluid inclusions from Pasir Manggu, Cibak, and Cileuweung.

inclusions, reflecting the hypabyssal inclusion characteristics of low-temperature hydrothermal-type gold deposits. However, compared with some typical shallow low-temperature hydrothermal deposits (White and Hedenquist, 1995), these aqueous inclusions have higher homogenization temperatures and salinities (Table 5), especially compared with those fluid inclusions of several low-sulfur-type hypabyssal low-temperature hydrothermal gold deposits in the West Java area (Marcoux and Milési, 1994; Basuki et al., 1994; Eric and Jean, 1994; Milesi et al., 1999; Mega and Hiroharu, 2002). These aqueous inclusions have large differences in temperature and salinity without obvious characteristics of boiling inclusion, which do not appear to have low-sulfur hypabyssal characteristics of low-temperature hydrothermal gold deposits, being almost equivalent to some typical high-sulfur epithermal deposits and porphyry deposits (Bonham, 1986; Carrillor et al., 2003; Heald et al., 1987). Thus, we suggest that the fluid inclusions in Ciemas are characterized by both high-sulfur epithermal gold deposits and porphyry deposits. Other studies also indicate that the porphyry deposits and shallow low-temperature hydrothermal deposits are closely related in time and space. Our study on fluid inclusions reflects this characteristic (Hedenquist et al., 1998; Qin et al., 2002; Sillitoe, 1997).

In addition, the gas/liquid ratios change little in Ciemas, and the fluid inclusion in quartz has no obvious boiling characteristics. The fluid inclusion salinity increases with homogenization temperature (Fig. 14d), which can be explained by the fluid mixing mechanism (Gammons and Williams, 1997). In the Cipirit deposit, during the process of quartz diorite porphyrite intrusion, the magma chamber gave off fluids of low–medium salinity, which migrated under the action of heat rising along the magma passage, giving off dense fluids with high salinity (>25 wt.% NaCl) with enriched Au metal, and low fluid salinity with poor Au and enriched H_2S in the open structural parts of the porphyry bodies. The former fluid in the parent rock intrusion formed near porphyry sulfide-type and quartz vein-type gold deposits. The latter fluid passed into the shallow low-temperature zone, was mixed and heated in the presence of atmospheric water with lower salinity that was produced in the low-salinity, low-temperature fluid; this process resulted in argillic alteration in the fractural structures, transforming $AuCl_2^-$ into Au $(HS)_2^-$ in the fluid, the occurrence of a cooling process during tectonic activity, and dilution of Au deposition, which is similar to a typical porphyry contact zone for hypabyssal low-temperature hydrothermal gold deposits (Christoph, 2005).

7.4. Metallogenic mechanism and the trinity metallogenic model

Many researchers suggest that the epithermal and porphyry deposits are spatially and genetically related to the same magmatic hydrothermal systems (Corbett, 2002; Gammons and Williams, 1997; Muntean and Einaudi, 2001). The Ciemas Au deposit contains three different mineralization types of ore bodies, and the mineralization is

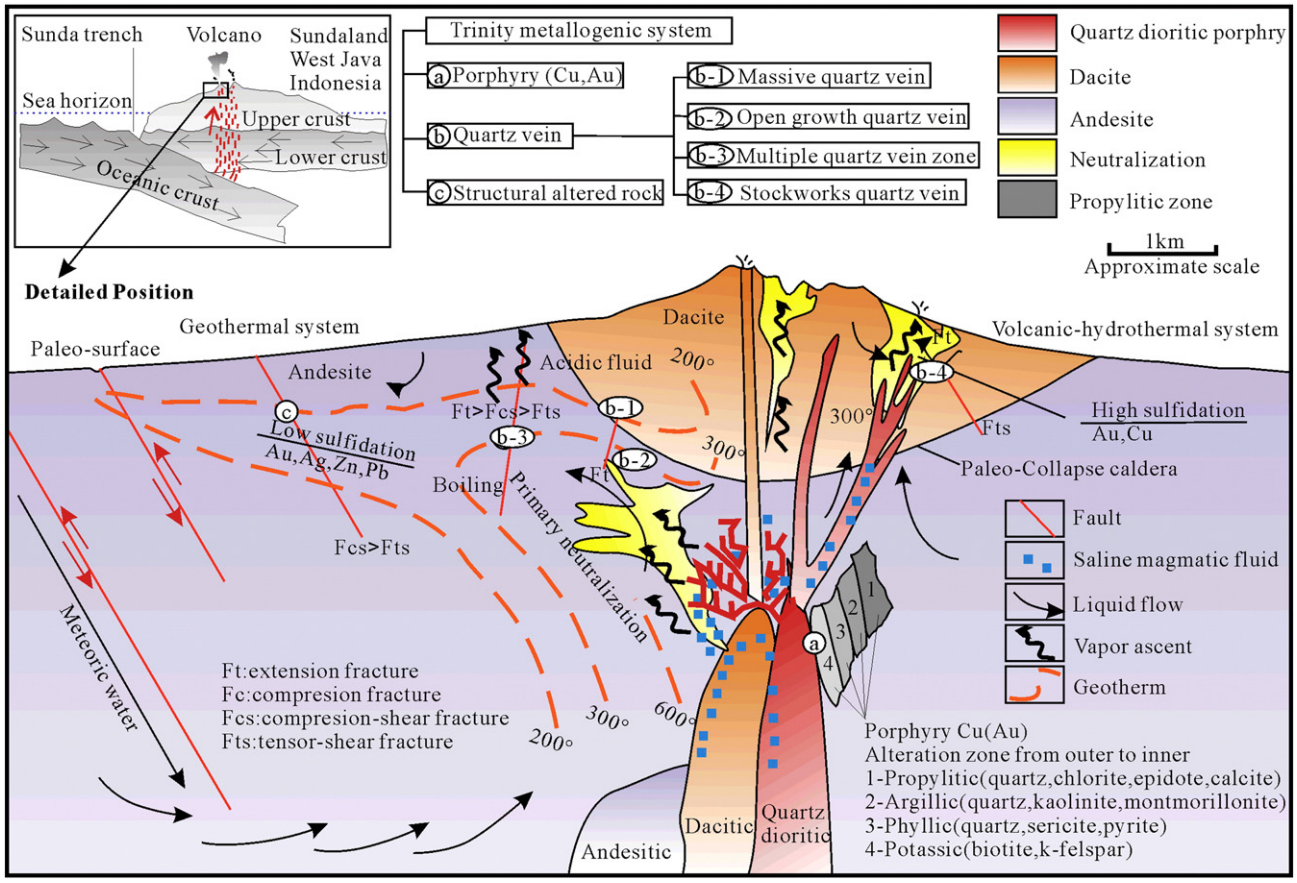

Fig. 15. The trinity model of the Au deposits with metallogenic porphyry, quartz vein and tectonically altered rocks of Ciemas, West Java, Indonesia.

related to quartz diorite porphyrite. Accordingly, we propose a descriptive geological–metallogenic model for its formation based on the geological and geochemical studies (Fig. 15).

During the Miocene (17–19 Ma), the southern margin of the Sunda continental arc volcanic magma activity frequently included large-scale andesitic eruptions, forming magma eruptions and developing a caldera structure system. With the further evolution of andesitic magma, the magma was intruded along the previous channel-formed dacite shaped in bedrock on the top of andesite, which was then intruded by a quartz diorite porphyrite intrusion shaped as a stock. Tectonically, after the eruption of andesite in the caldera system formed the high-angle extensional faults and then formed fractures having NE and NW directions, they underwent different degrees of extension, compression and shearing during multiple later tectonic movements, which provided the space for magmatic–hydrothermal residence.

In the porphyry bodies and contact zone, porphyry copper and gold deposits formed (Fig. 15a), whereas in the porphyry contacts, quartz vein-type gold bodies formed (Fig. 15b-4). In the fault belt of the caldera and contact zone between andesite and dacite, massive quartz vein-type deposits formed (Fig. 14b-1), and quartz vein-type deposition in the open environment occurred (Fig. 15b-2). In the fault belt on the fringes of the caldera, due to the high salinity from quartz diorite magma mixed with hydrothermal fluid from precipitation, compound vein quartz vein-type gold deposits formed (Fig. 15b-3). Structurally-controlled altered gold deposits formed in the fault belt far away from porphyry (Fig. 15c), which was caused by rock crushing, alteration and atmospheric precipitation as a result of the thermal cycle. Although these ore body mineralization types are different, they have internal relationships in terms of their genesis and “the trinity” in space.

8. Conclusions

1) The Cipirit quartz diorite porphyrite formed in the Miocene, where porphyry, quartz–sulfide vein type and tectonic altered-type gold deposits formed in the inner and outer contact zones of different tectonic zones. Their ore-forming mechanisms are related to late magmatic evolution within a thermodynamic system.
2) The Ciemas deposit is a typical example that was derived from the volcanic hydrothermal and shallow surface of the plate subduction zone. Not only is this deposit characterized by enrichment in ore-forming elements, but it also developed ore-forming parent materials, and the derived thermodynamic ore-forming fluid migrated to the tectonic zones, enabling the formation of different types of gold deposits.
3) Finally, we have explained the regional metallogenic model responsible for the formation of these deposits in the magmatic hydrothermal system and geothermal system containing meteoric water.

Acknowledgments

The research was financially supported by the Natural Science Foundation of China (NSFC Nos. 41090372; 41173064; 913282009) and the 12th Five-Year Plan project of State Key Laboratory of Ore-deposit Geochemistry, Chinese Academy of Sciences (SKLODG-ZY125-08). Mr. Wijaya Lawrence provided invaluable support for field trips and exploration data. The authors are grateful to Prof. Franco Pirajno and Prof. Chen Yanjing for their helpful suggestions about an early version of this manuscript.

Appendix A. Supplementary data

Supplementary data associated with this article can be found in the online version, at http://dx.doi.org/10.1016/j.oregeorev.2014.07.003. These data include Google maps of the most important areas described in this article.

Appendix A. Supplementary data

Supplementary data to this article can be found online at http://dx.doi.org/10.1016/j.oregeorev.2014.07.003.

References

Basuki, A., Aditya, S.D., Sinambela, D., 1994. The Gunung–Pongkor gold–silver deposit, West Java, Indonesia. J. Geochem. Explor. 50, 371–391.

Bemmelen, R.W., 1949. The Geology of Indonesia. US Government Printing Office.

Bemmelen, R.W., 1970. The Geology of Indonesia. Martinus Nijhoff, pp. 1–30.

Berger, B.R., 1983. The relationship of alteration and trace element patterns. Special Report Geothermal Resources Council, 13, p. 255.

Bodnar, R.J., 1993. Revised equation and table for determining the freezing point depression of H_2O–NaCl solutions. Geochim. Cosmochim. Acta 57 (3), 683–684.

Bonham, H.F., 1986. Models for volcanic-hosted epithermal precious metal deposits: a review. International Volcanological Congress, Symposium 5. Volcanism, Hydrothermal Systems and Related Mineralization., pp. 13–17 (Hamilton, New Zealand, February).

Brown, P.E.F., 1989. A microcomputer program for the reduction and investigation of fluid inclusion data. Am. Mineral. 74, 1390–1393.

Brown, P.E., Lamb, W.M., 1989. P–V–T properties of fluids in the system $H_2O \pm CO_2 \pm NaCl$: new graphical presentations and implications for fluid inclusion studies. Geochim. Cosmochim. Acta 53 (6), 1209–1221.

Buchanan, L.J., 1981. Precious metal deposits associated with volcanic environments in the southern Cordillera. In: Dickinson, W.R., Payne, W.D. (Eds.), Arizona Geological Society digest, p. 14.

Carlile, J.C., Mitchell, A.H.G., 1994. Magmatic arcs and associated gold and copper mineralization in Indonesia. In: Leeuwen, T.M., Hedenquist, J.W., James, L.P., Dow, J.A.S. (Eds.), Indonesian mineral deposits — discoveries of the past 25 years. Journal Geochemical Exploration, 50, pp. 91–142.

Carrillor, R.F.J., Morales, R.S., Boyce, A.J., 2003. High and intermediate sulphidation environment in the same hydrothermal deposit: the example of Au–Cu Palai–Islica deposit, Carboneras. In: Eliopoulos, et al. (Eds.), Proceedings of the Seventh Biennial SGA Meeting: Mineral Exploration and Sustainable Development. Millpress Science Publishers, Rotterdam, pp. 445–448.

Christoph, A.H., 2005. The physical and chemical evolution of low-salinity magmatic fluids at the porphyry to epithermal transition: a thermodynamic study. Mineral. Deposita 39, 864–889.

Claproth, R., 1989. Magmatic rocks from Ungaran, Central Java. Geol. Indones. 12, 511–562.

Clements, B., Hall, R., 2007. Cretaceous to late Miocene stratigraphic and tectonic evolution of West Java. Proceedings, Indonesian Petroleum Association. Thirty-First Annual Convention and Exhibition, IPA07-G-037.

Clements, B., Hall, R., 2008. U–Pb dating of detrital zircons from West Java show complex Sundaland provenance. Proceedings, Indonesian Petroleum Association. Thirty-First Annual Convention and Exhibition, IPA08-G-115.

Cooke, D.R., McPhail, D.C., 2001. Epithermal Au–Ag–Te mineralization, Acupan, Baguio District, Philippines, numerical simulations of mineral deposition. Econ. Geol. 96, 109–131.

Corbett, G., 2002. Epithermal gold for explorationists. AIG Journal Applied Geoscientific Practice and Research in Australia 1–26 April.

Davies, A.G.S., Cooke, D.R., Gemmell, J.B., et al., 2003. The Kelian breccia complex: a giant epithermal gold–silver deposit in Kalimantan, Indonesia. In: Eliopoulos (Ed.), Proceedings of the Seventh Biennial SGA Meeting: Mineral Exploration and Sustainable Development. Millpress Science Publishers, Rotterdam, pp. 465–468.

De, H.J., Mason, P., Van, B.M., 2001a. Sulfur and chalcophile elements in subduction zones: constraints from a laser ablation ICP-MS study of melt inclusions from Galunggung Volcano, Indonesia. Geochim. Cosmochim. Acta 65, 3147–3164.

De, H.J., Taylor, B., Van, B.M., 2001b. Sulfur isotope systematics of basaltic lavas from Indonesia: implications for the sulfur cycle in subduction zones. Earth Planet. Sci. Lett. 189, 237–252.

Deyell, C.L., Cooke, D.R., et al., 2003. Mineralogical and isotopic evidence for the genesis of the Kelly gold–silver deposit, Baguio District, Philippines: diverse mineral assemblages in an evolving epithermal system. In: Eliopoulos (Ed.), Proceedings of the Seventh Biennial SGA Meeting: Mineral Exploration and Sustainable Development. Millpress Science Publishers, Rotterdam, pp. 469–472.

Eric, M., Jean, P.M., 1994. Epithermal gold deposits in West Java, Indonesia: geology, age and crustal source. J. Geochem. Explor. 50, 393–408.

Gammons, C.H., Williams, J.A.E., 1997. Chemical mobility of gold in the porphyry–epithermal environment. Econ. Geol. 92, 45–59.

Hall, R., 2002. Cenozoic geological and plate tectonic evolution of SE Asia and the SW Pacific: computer-based reconstructions, model and animations. J. Asian Earth Sci. 20, 353–434.

Hamilton, W., 1988. Plate tectonics and island arcs. Geol. Soc. Am. Bull. 100, 1503–1527.

Hamilton, W., 1989. Convergent-plate tectonics viewed from the Indonesia region. Geology Indonesia 12, 35–88.

Heald, P., Foley, N.K., Hayba, D.O., 1987. Comparative anatomy of volcanic-hosted epithermal deposits — acid sulphate and adularia–sericite types. Econ. Geol. 80, 1–26.

Hedenquist, J.W., Arribas, A.J., Reynolds, T.J., 1998. Evolution of an intrusion-centered hydrothermal system: Far Southeast Lepanto porphyry and epithermal Cu–Au deposits, Philippines. Econ. Geol. 93, 373–404.

Hedenquist, J.W., Arribas, R.A., Gonzalez, U.E., 2000. Exploration for epithermal gold deposits. Econ. Geol. 13, 245–277.

Heinrich, C.A., 2005. The physical and chemical evolution of low-salinity magmatic fluids at the porphyry to epithermal transition: a thermodynamic study. Mineral. Deposita 9, 864–889.

Heinrich, C.A., Driesner, T., Stefansson, A., 2004. Magmatic vapor contraction and the transport of gold from porphyry to epithermal ore deposits. Geology 32, 761–764.

Hong, G., Falong, H., Muhui, H., Richard, K., Yuanhai, L., Jinhui, L., Pengfei, X., et al., 2013. Independent Qualified Person's Report for the Ciemas Gold Project, Ciemas, Sukabumi Region, Republic of Indonesia (Project Number: SHK191).

Hu, Z.C., Liu, Y.S., Chen, L., Zhou, L., Li, M., Zong, K.Q., Zhu, L.Y., Gao, S., 2011. Contrasting matrix induced elemental fractionation in NIST SRM and rock glasses during laser ablation ICP-MS analysis at high spatial resolution. J. Anal. At. Spectrom. 26, 425–430.

Hutchison, C.S., 1988. The tin metallogenic provinces of Southeast Asia and China: a Gondwanaland inheritance. In: Hutchison, C.S. (Ed.), Geology of Tin Deposits in Asia and the Pacific. Springer Verlag, pp. 225–235.

Jonathan, M.N., 2007. Ciemas prospect West Java, Indonesia geological evaluation study. Jakarta: Geological Report, pp. 1–46.

Katili, J.A., 1975. Volcanism and plate tectonics in the Indonesian island arcs. Tectonophysics 26, 165–188.

Katili, J.A., 1989. Evolution of the southeast Asian arc complex. Geology Indonesia 21, 113–143.

Lindgren, W., 1933. Mineral Deposits, 4th ed. McGraw Hill, New York, pp. 1–930.

Liu, B., Duan, G.X., 1987. The density and isochoric formulae for NaCl–H_2O fluid inclusions and their applications. Acta Mineral. Sin. 7, 345–351 (in Chinese with English abstract).

Liu, Y.S., Gao, S., Hu, Z.C., Gao, C.G., Zong, K.Q., Wang, D.B., 2010a. Continental and oceanic crust recycling-induced melt–peridotite interactions in the Trans-North China Orogen: U–Pb dating, Hf isotopes and trace elements in zircons from mantle xenoliths. J. Petrol. 51, 537–571.

Liu, Y.S., Hu, Z.C., Zong, K.Q., Gao, C.G., Gao, S., Xu, J., Chen, H.H., 2010b. Reappraisement and refinement of zircon U–Pb isotope and trace element analyses by LA–ICP-MS. Chin. Sci. Bull. 55, 1535–1546.

Lu, Y.F., 2004. GeoKit: a geochemical toolkit for Microsoft Excel. Geochemica 33, 459–464 (in Chinese with English abstract).

Ludwig, K.R., 2003. User's Manual for Isoplot 3.00, A Geochronological Toolkit for Microsoft Excel. Berkeley, CA, Berkeley Geochronology Center Special, Publication, 4, p. 67.

Marcoux, E., Milési, J.P., 1994. Epithermal gold deposits in west Java, Indonesia: geology, age and crustal source. J. Geochem. Explor. 50, 393–408.

Mega, F.R., Hiroharu, M., 2002. Cikidang hydrothermal gold deposit in West Java, Indonesia. Resour. Geol. 52 (4), 341–352.

Milesi, J.P., Marcoux, E., Sitorus, T., 1999. Pongkor (west Java, Indonesia): a Pliocene supergene-enriched epithermal Au–Ag–(Mn) deposit. Mineral. Deposita 34 (2), 131–149.

Muntean, J.L., Einaudi, M.T., 2001. Porphyry–epithermal transition: Maricunga Belt, northern Chile. Econ. Geol. 96, 743–772.

Nicholls, I., Whitford, D., Harris, K., Taylor, S., 1980. Variation in the geochemistry of mantle sources for tholeiitic and calc-alkaline mafic magmas, western Sunda volcanic arc, Indonesia. Chem. Geol. 30, 177–199.

Palme, H., O'Neill, H.S.C., 2003. Cosmochemical estimates of mantle composition. Treatise on Geochemistry 2, 1–38.

Qin, K.Z., Sun, S., Li, J.L., 2002. Paleozoic epithermal Au and porphyry Cu deposits in North Xinjiang, China: epochs, features, tectonic linkage and exploration significance. Resour. Geol. 52 (4), 291–300.

Sillitoe, R.H., 1997. Characteristics and controls of the largest porphyry copper–gold and epithermal gold deposits in the circum-Pacific region. Aust. J. Earth Sci. 44, 373–388.

Soeria, A.R., Maury, R., Bellon, H., Pringgo, H., Polve, M., Priadi, B., 1994. Tertiary magmatic belts in Java. J. SE Asian Earth Sci. 9, 13–27.

Sukamto, R., 1975. Geologic map of the Jampang and Balekambang quadrangles, Java (Quadrangles 9–XIV–A, 8–XIV–C): Scale 1:100,000, Geological research and development centre, Bandung 11, pp.1.

Van, B.R.W., 1970. The Geology of Indonesia: The Hague, Martinus Nijhoff, v.2, p. 732.

Wakita, K., 2000. Cretaceous accretionary–collision complexes in central Indonesia. J. Asian Earth Sci. 18, 739–749.

White, N.C., Hedenquist, J.W., 1995. Epithermal gold deposits: styles, characteristics and exploration. SEG Newsl. 23 (1), 9–13.

Whitford, D.J., Nicholls, I.A., Taylor, S.R., 1979. Spatial variations in the geochemistry of Quaternary lavas across the Sunda arc in Java and Bali. Contrib. Mineral. Petrol. 70, 341–356.

Xu, J.H., Zhang, G.R., Wei, H., 2012. Ore-forming pressures and depths of vein gold deposit: fluid inclusions studies and their influence factors. J. Nanjing Univ. 48, 266–277 (in Chinese with English abstract).

Zhou, W.D., Zhang, Z.W., Wang, G.W., Wu, C.Q., Li, Y.J., 2014. Characteristics and mineralization epochs of the Bairong porphyry copper–molybdenum deposit in the Nyemo County, Tibet. Bull. Mineral. Petrol. Geochem. 33, 77–184 (in Chinese with English abstract).